

MASARYKOVA UNIVERZITA
Přírodovědecká fakulta
Ústav teoretické fyziky a astrofyziky

Diplomová práce

Brno 2021

Jakub Kolář

MASARYKOVA UNIVERZITA
Přírodovědecká fakulta
Ústav teoretické fyziky a astrofyziky

Diplomová práce

Studium vybraných oddělených
zákrytových dvojhvězd

Jakub Kolář

Vedoucí práce:
doc. RNDr. Miloslav Zejda, Ph.D.

Brno 2021

Bibliografický záznam

Autor: Jakub Kolář
Přírodovědecká fakulta, Masarykova univerzita
Ústav teoretické fyziky a astrofyziky

Název práce: Studium vybraných oddělených zákrytových dvojhvězd

Studijní program: Fyzika

Studijní plán: Astrofyzika

Vedoucí práce: doc. RNDr. Miloslav Zejda, Ph.D.

Akademický rok: 2020/2021

Počet stran: IX + 86

Klíčová slova: Zákrytové dvojhvězdy, CCD fotometrie, světelná křivka, křivka radiálních rychlostí, $O - C$ diagram

Bibliographic Entry

Author: Jakub Kolář
Faculty of Science, Masaryk University
Department of Theoretical Physics and Astrophysics

Title of Thesis: Study of selected detached eclipsing binaries

Degree Programme: Physics

Study Plan: Astrophysics

Supervisor: doc. RNDr. Miloslav Zejda, Ph.D.

Academic Year: 2020/2021

Number of Pages: IX + 86

Keywords: Eclipsing binaries, CCD photometry, light curve, radial velocity curve, $O - C$ diagram

Abstrakt

Tato práce pojednává o studiu čtyř zákrytových dvojhvězd typu B: GX Lac, TT Lyr, OGLE LMC-ECL-7641 a OGLE LMC-ECL-17660. Pro tyto systémy byla zorganizována pozorovací kampaň za účelem získání nových fotometrických dat. Další fotometrická a spektroskopická měření byla převzata z dostupných přehlídek a databází. Pro každou hvězdu byla provedena periodová analýza a byly sestrojeny světelné křivky a křivky radiálních rychlostí. V programu PHOEBE byly vypočteny modely těchto systémů, ze kterých byly získány absolutní parametry hvězd a následně byla určena jejich vzdálenost.

Abstract

This thesis deals with the study of four eclipsing binary B-type stars: GX Lac, TT Lyr, OGLE LMC-ECL-7641, and OGLE LMC-ECL-17660. An observation campaign was organized for these systems to obtain new photometric data. Other photometric and spectroscopic measurements were taken from available surveys and databases. Period analysis was performed for each star and the light curves and the radial velocity curves were constructed. Models of these systems were calculated in PHOEBE software and then their distances were determined.

ZADÁNÍ
DIPLOMOVÉ PRÁCE

Akademický rok: 2019/2020

Ústav:	Ústav teoretické fyziky a astrofyziky
Student:	Bc. Jakub Kolář
Program:	Fyzika
Obor:	Astrofyzika

Ředitel Ústavu teoretické fyziky a astrofyziky PŘF MU Vám ve smyslu Studijního a zkušebního řádu MU určuje diplomovou práci s názvem:

Název práce:	Studium vybraných oddělených zákrytových dvojhvězd
Název práce anglicky:	Study of selected detached eclipsing binaries

Oficiální zadání:

Oddělené těsné dvojhvězdy představují zcela jedinečný zdroj informací o hvězdách. Umožňují zejména přesné určení hmotností složek a dalších parametrů, které následně vedou až k určení vzdáleností sledovaných dvojhvězd. V rámci diplomové práce se student zaměří na dva oddělené zákrytové systémy s podobnými vlastnostmi, jeden v naší Galaxii a jeden v jiné galaxii. Na základě analýzy vlastních a převzatých fotometrických a spektroskopických pozorování určí parametry dvojhvězd a jejich složek a provede jejich srovnání.

Literatura:

PRŠA, Andrej. *Modeling and analysis of eclipsing binary stars : the theory and design principles of PHOEBE*. Bristol: IOP Publishing, 2018. xiv, 199. ISBN 9780750312882.

Jazyk závěrečné práce:	angličtina
Vedoucí práce:	doc. RNDr. Miloslav Zejda, Ph.D.
Datum zadání práce:	12. 11. 2019
V Brně dne:	12. 11. 2019

Souhlasím se zadáním (podpis, datum):

.....
Bc. Jakub Kolář
student

.....
doc. RNDr. Miloslav Zejda, Ph.D.
vedoucí práce

.....
prof. Rikard von Unge, Ph.D.
ředitel Ústavu teoretické fyziky a
astrofyziky

Poděkování

Rád bych na tomto místě poděkoval svému školiteli doc. RNDr. Miloslavu Zejdovi, Ph.D. za vstřícný přístup a cenné rady při konzultacích. Děkuji také Ing. Reinholdu Auerovi za velkou ochotu podílet se na pozorovací kampani. Dále bych chtěl poděkovat Mgr. Marku Skarkovi, Ph.D. za pomoc při uskutečnění spektroskopických pozorování v Ondřejově a RNDr. Janu Janíkovi, Ph.D. za cenné rady při analýze spekter.

Prohlášení

Prohlašuji, že jsem svoji diplomovou práci vypracoval samostatně pod vedením vedoucího práce s využitím informačních zdrojů, které jsou v práci citovány.

Brno 4. června 2021

.....

Jakub Kolář

Contents

1	Eclipsing Binary Stars	1
1.1	Introduction	1
1.2	Types	2
1.2.1	Light Curves	2
1.2.2	Morphological Classification	3
1.3	Evolution	4
1.4	Large Magellanic Cloud	6
2	CCD Photometry	8
2.1	CCD	8
2.2	Correction Frames	9
2.3	Photometric Filters	10
2.3.1	Colour Index	11
2.4	Data Analysis	12
2.4.1	Light Curve	12
2.4.2	Timings of the Minima	13
2.4.3	$O - C$ Diagram	14
3	Spectroscopy	18
3.1	Introduction	18
3.2	Spectral Classification	18
3.2.1	Spectral Type B	20
3.3	Measuring	20
3.4	Radial Velocities	21
4	Selected objects	24
4.1	Basic Information	24
4.1.1	GX Lac	24
4.1.2	TT Lyr	25
4.1.3	OGLE LMC-ECL-7641	26
4.1.4	OGLE LMC-ECL-17660	26

4.2	Observations	27
4.2.1	Photometry	27
4.2.2	Spectroscopy	29
5	Data Analysis	32
5.1	Period Analysis	32
5.2	Light Curves	39
5.3	Radial Velocities	42
5.4	Modelling	45
5.5	Discussion	57
	Conclusion	60
	Bibliography	62
	Appendices	71

Chapter 1

Eclipsing Binary Stars

1.1 Introduction

The binary system consists of two stars, which are gravitationally bound and orbit their common centre of mass. This motion occurs along a circular or elliptical trajectory. Orbital periods of these systems are very diverse. The shortest measured periods can reach values in the order of minutes¹, the highest known periods are up to dozens of years².

If the orbital plane of the system is the same or close to the plane of the observer, the stars may eclipse each other viewing from the Earth. The eclipses cause periodical decreases in the total brightness of the stellar system. The period of the brightness changes is the same as the orbital period. Inclination angle i means the angle between the normal to the orbital plane and the direction to the observer. The condition for viewing the eclipses can be expressed as follows (Hilditch 2001):

$$\sin(90^\circ - i) \geq \frac{R_1 + R_2}{r}, \quad (1.1)$$

where r is the distance between the stars and R_1 and R_2 are their radii. The angle i is typically close to 90 deg.

Orbiting the centre of gravity, one component eclipse the other. After half of the period, a situation reverses. In both cases, the brightness of the system first decreases, then reaches a minimum, and finally rises again to the original brightness before the eclipse. The minima are divided into primary and secondary. Usually, the primary minimum is with a greater decrease in magnitude. The time dependence of brightness can be plotted in a graph called a *light curve*.

¹ZTF J153932.16+502738.8: aavso.org/vsx/index.php?view=detail.top&oid=844294

²AS LMi: aavso.org/vsx/index.php?view=detail.top&oid=297394

The time on the horizontal axis is usually in Julian dating. In most cases, magnitude or flux is on the vertical axis of the light curve.

Binary stars belong to the group of the extrinsic variable stars. Variability is caused by geometry of individual objects. There are no luminosity changes unless there are other causes of variability. For astrophysical research, binary stars are extremely important. They can bring more knowledge of stellar formation and evolution. The parameters of the components of a binary star system can be determined. In particular, it is possible to determine the mass of the stars, which is an often difficult task. Using the calculated parameters, it is possible to derive the system distance. Binary stars can thus be used to determine distances in the Universe (e.g. star clusters or galaxies) independently to other methods. For multiple star systems, where the stars form subsystems, and extrasolar planetary systems, the mechanics of the binary stars can also be applied.

1.2 Types

1.2.1 Light Curves

Eclipsing variable stars are historically grouped into three classes: Algol-type variables (EA), β Lyrae systems (EB), and W UMa systems (EW). Their names are reflected by the most known representatives of each type. This classification follows from the shape of the light curve and tells about some characteristics of the binary stars (see Figure 1.1). The similar light curves may be the result of eclipses of different objects. The shape of the light curve does not clearly indicate the nature of the components.

Algol-type eclipsing binaries have typically sharp and narrow minima. A secondary minimum is usually shallower than the primary. The secondary minimum does not be visible evidently. Outside the eclipses, brightness remains mostly constant. This appearance of the light curve indicates a detached system (section 1.2.2). However, the stars can interact with each other in certain cases. For Algol itself, a less bright component is such evolved, that it has filled its Roche lobe, and transfers matter to its companion. The orbital periods of these stars are very diverse. The longest orbital periods could be dozens of years.

Light curves of β Lyrae type stars are characterized by continuous variability of luminous flux. These changes of brightness lead to considerations of the ellipsoidal shape of the stars. The minima represent a significant part of the periodic cycle. Different depths of the minima suggest that components differ in surface brightness. The orbital periods are usually longer than 0.5 days.

Similar to the previous class, the brightness of W UMa binaries varies continuously. Both minima are similar. Such systems consist of ellipsoidal stars that

could be in physical contact or even have a common envelope. Typically, the period values of W UMa variables are less than a day.

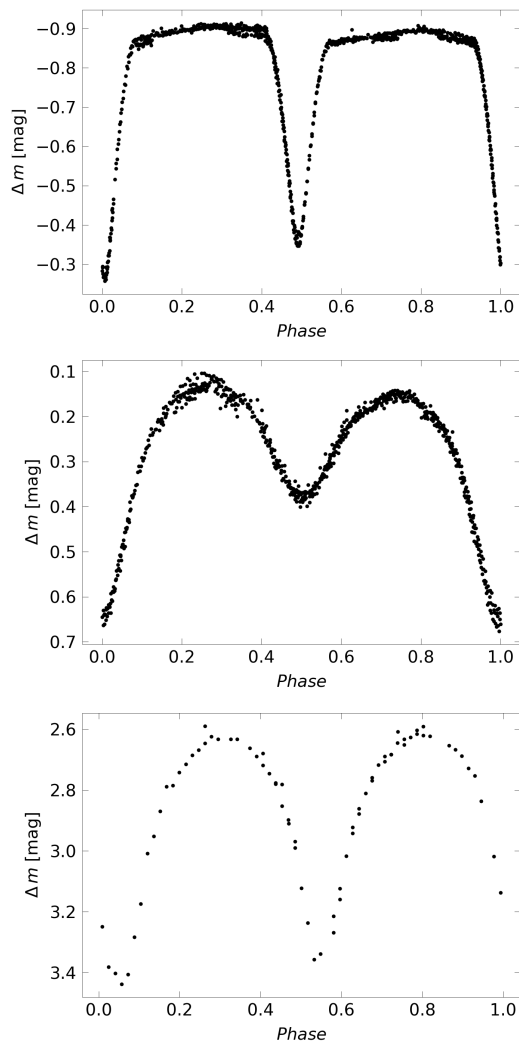


Figure 1.1: Examples of types of eclipsing binary stars based on the shape of the light curve, from top to bottom: CO Lac (Algol type), V474 Lac (β Lyrae type), and BM UMa (W UMa type). The observations were made at the observatory on Kraví hora in Brno by J. Kolář.

1.2.2 Morphological Classification

The gravitational potential around a single star depends on the inverse value of the distance from the centre of the star. Surfaces with the same gravitational

potential are called equipotential surfaces and are spherically symmetrical for isolated objects without significant gravitational influences. For binary stars, the shape of the equipotential surfaces depends on the mass ratio of the binary components. The special case of equipotential surfaces is the Roche surface or otherwise called critical surface. It defines Roche lobes around both components. The lobes touch at Lagrange libration point L_1 at an angle of about 115° . The size of the Roche lobe depends on the star masses, radii, and the distance between the components. An approximate relation in Eggleton (1983) gives the radius R_1 of the sphere with the Roche lobe volume:

$$\frac{R_1}{a} = \frac{0.49 q^{\frac{2}{3}}}{0.6 q^{\frac{2}{3}} + \ln\left(1 + q^{\frac{1}{3}}\right)}. \quad (1.2)$$

The relation applies to the component with mass M_1 , mass ratio $q = M_2/M_1$, and the distance a between the stars. According to the degree of filling of the Roche lobe by the star, Kopal (1955) introduced a classification for close binaries. Modified and supplemented, it is still used today.

For *detached* binaries, both stars are well within their Roche lobes. The tidal forces between the components are insignificant and the stars have an approximately spherical shape (Percy 2007). In *semidetached* systems, one star has filled its Roche lobe and can transfer material to the other component through the Lagrangian point L_1 . If both stars fill the space bounded by their Roche lobes, they are referred to as *contact* binaries. In this type, the matter is transferring between the components. In some cases, the stars may even extend beyond the Roche lobes and have a common envelope. These objects are called *overcontact* binaries. Wilson (1979) supplemented this classification with a type of *double-contact* stars. Such stars precisely fill their lobes, but they do not touch each other. The instances of binary star types, according to this classification, are shown in Figure 1.2.

1.3 Evolution

In the centre of main-sequence stars, nuclear reactions are underway. Hydrogen is converted to helium. There is not only one reaction but a sequence of multiple reactions. The *proton-proton chain* is energetically dominant for the stars on the main sequence, whose mass is less than around $2 M_\odot^3$. The *CNO cycle*, where carbon, nitrogen, and oxygen enter into the reactions as catalysts, prevails for more massive stars. The star will spend the longest time of its existence on the main sequence. Main-sequence epoch of star life strongly depends

³Solar mass $M_\odot \approx 1.989 \times 10^{30}$ kg

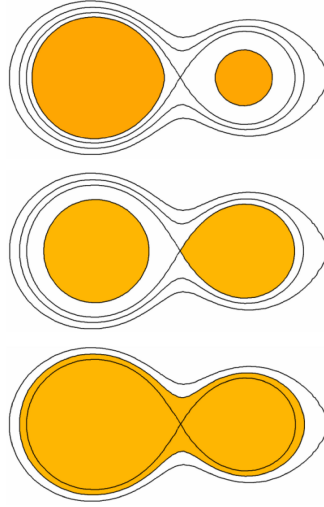


Figure 1.2: Schemes of the binary systems according to their morphological classification, from top to bottom: detached, semi-detached and overcontact (Terrell 2001).

on the initial mass of the star. The more mass, the time on the main sequence is shorter and the evolution of the star is faster.

The stars with masses between $0.5 M_{\odot}$ to $11 M_{\odot}$ move on the HR diagram away from the main sequence into the red giants region after the almost complete depletion of hydrogen fuel in the centre. The red giant throws away its upper parts and a planetary nebula is created. The remaining core is a white dwarf. This phase leads to yet undiscovered and hypothetical black dwarf. More massive stars end their life in an explosion as a supernova. After that there could be two scenarios: a neutron star, or a black hole (if the initial mass is higher than $50 M_{\odot}$). The less massive stars than $0.5 M_{\odot}$ gradually cool and get directly into the black dwarf phase.

The evolution of close binary systems differs significantly from the evolution of single stars. Binary and multiple stars are mostly formed from the same original molecular cloud. It means that the components of the multiple star system are the same age and have the same initial chemical composition. The evolution of more massive stars is faster and the stars expand earlier than less massive components. The volumes of the expanded stars in binary systems are limited by their Roche lobes which are non-spherical.

The components on the main sequence evolve independently as if they were single stars. A more massive star (primary) is evolving faster. It will expand earlier and fill its Roche lobe. The mass from the outer parts of the star begins to flow through the point L_1 to the secondary component, a rapid mass exchange

phase occurs (Plavec 1968). The angular momentum is also transferring along with the mass. A period of the system is shortening. For the mass transfer, a conservative overflow (Eggleton 2006) can be assumed. The total mass M and also the total angular momentum \mathcal{L} are constant. It can be assumed that the matter does not escape from the system.

A substantial part of the mass moves to the secondary component, which becomes more massive. The evolution of the primary component, however, continues as if it has not lost any matter. The evolution is influenced by the central parts of the star, which were not affected by the overflow of matter. The next phase of mass transfer is slow. Deceleration of the overflow occurs because the components move away from each other. As a result, the circulation period of the system increases. At the end of this phase, a main-sequence star and a subgiant are the components in the system.

In many cases, such as the star Algol itself, it is possible to observe the stars, that do not seem to correspond to the theory of stellar structure and evolution. In these systems, there is a more massive main-sequence star and less massive (sub)giant. It means, that less massive component is more evolved in these star systems. This situation is called the *Algol paradox*. The explanation for this phenomenon lies precisely in the overflow of matter from the originally more massive star to the less massive one.

Further evolution depends on the initial mass of both stars. For each component, one of the final stages (white dwarf, neutron star, or black hole) is possible. Various combinations can occur e.g. binary neutron star system (Portegies Zwart & Yungelson 1998). During the evolution of the secondary component, which was originally less massive, the system may completely disintegrate. The stars could also merge together.

1.4 Large Magellanic Cloud

Large Magellanic Cloud (LMC) is the closest galactic companion to our Galaxy. Together with, for instance, the galaxies M31, M33, and Small Magellanic Cloud (SMC) are part of The Local Group of galaxies. Both Magellanic Clouds are located in the southern hemisphere and are visible to the naked eye. LMC ranks among irregular dwarf galaxies. A faint sign of a galactic bar is observed there.

Thanks to its orientation, the LMC can be observed almost perpendicular to the Earth. Due to this fact and also the relatively small distance from the Galaxy, many of its objects can be studied well in depth. This galaxy thus enables the study of stars, their properties, and also interstellar medium. It also serves as an indicator of extragalactic distances. Using accurate distance mea-

measurements of the objects of LMC can then be used to calibrate the distance scale.

The distance of the Large Magellanic Cloud can be determined by several diverse methods e.g. from the Cepheids (Keller & Wood 2002, Alves 2004). In general, these methods may not give the same results and, in particular, the same measurement uncertainties (Ribas 2004). Using precise and detailed analysis of the eclipsing binary stars, with double line spectra, the distance determination can be very accurate. Pietrzyński et al. (2019) derived the LMC distance with an accuracy of 1 % from the distance of twenty eclipsing binary systems. For determine the distance, one needs light curves from photometry, radial velocity curves from spectroscopy, and additional information about interstellar reddening and temperatures of the stars (Ribas 2004).

Chapter 2

CCD Photometry

2.1 CCD

Photometry is one of the oldest and most significant observational methods in astronomy. The main task of photometric observations is to measure the luminous flux coming from cosmic objects. In addition to the human eye, which is a very subjective detector of radiation, photographic cameras, and photomultipliers were mainly used for photometry. Currently, most of these observations are carried out using CCD cameras.

The CCD component (Charged Coupled Device) was invented in 1969 at the Bell Laboratories (Boyle & Smith 1970). The first CCD camera was introduced the following year. The CCD chip consists of a silicon plate which is composed of a matrix of light-sensitive elements. These elements are called pixels, and their dimensions are of the order of micrometers. The incoming photons that reach the surface of the chip release electrons from silicon atoms through the photoelectric effect. The electrons are then maintained in the pixels, which act as potential wells with the help of an electrode system.

After completing the exposure the captured charge is converted into an electrical signal. The amount of signal in each pixel is given in ADU (Analog to Digital Unit). The dynamic range of the CCD camera is determined by the A/D converter. For the most commonly used 16-bit converter, the dynamic range is 65 536 ADU (from 0 to 65 535 ADU). When the pixel is saturated, the electrons overflow from the potential well and affect the surrounding pixels. This effect is called *blooming*. It can be removed using other electrodes, which divert the excess electrons away (*anti-blooming*). The data are saved as image files in the FITS (Flexible Image Transport System) format (Wells & Greisen 1979). Each file also contains a header with information about the image.

The CCD element is generally very sensitive, which allows observing very faint objects. Within one observation, a large number of stars can be captured in the image at once. During processing CCD frames, comparison and check stars are selected. These stars should be the same magnitude and spectral type as the measured variable star. Usually, there is no issue finding suitable stars for comparison on a captured star field. A great advantage of CCD photometry is the possibility to return to the images at any time and make a new measurement. An important property of a CCD camera is the linearity of the chip, the output signal is directly proportional to the number of photons. Quantum efficiency is the ratio between registered and incident photons. CCD detectors have it many times higher than other photometric devices. Typical values of the quantum efficiency of CCD cameras are tens of percent, the most sensitive chips have more than 90 % (Howell 2006, Sperlich & Stolz 2013).

2.2 Correction Frames

The raw images have to be adjusted before the analysis because they contain a lot of defects. Due to the thermal motion of electrons, thermal noise is generated. It creates a dark current, which is directly proportional to the exposition time and depends also on the temperature of the chip. The CCD camera is usually cooled down to the temperature 20 to 30 K lower than ambient temperature. Despite the cooling, the dark current is still significant in the obtained images.

To eliminate the dark current, a *dark frame* is taken. This frame is obtained with the same temperature and exposition time as the data (light) image but with a closed shutter. Usually, a series of several dark frames are taken, which are then combined by a median into one final image called the masterdark. The noise is removed by subtracting the masterdark from the data frames.

Generally, each pixel of the camera is differently sensitive. The image can be also affected by vignetting, dusts, dirt on the optics that spoil the resulting image. These deviations are removed by a *flat field* frame. To obtain the flat field, a clear sky is captured during twilights. Alternatively, an evenly lit area can be used. Several frames are corrected by masterdark and combined into one masterflat frame. These correction frames have to be photographed separately for each filter because the sensitivity of the camera differs in distinct areas of the spectrum and each filter could have its defects and dirt.

Before calculation of star photometry and further analysis each data (light) frame is subtracted by masterdark and divided by masterflat images. Examples of correction frames are shown in Figure 2.1.

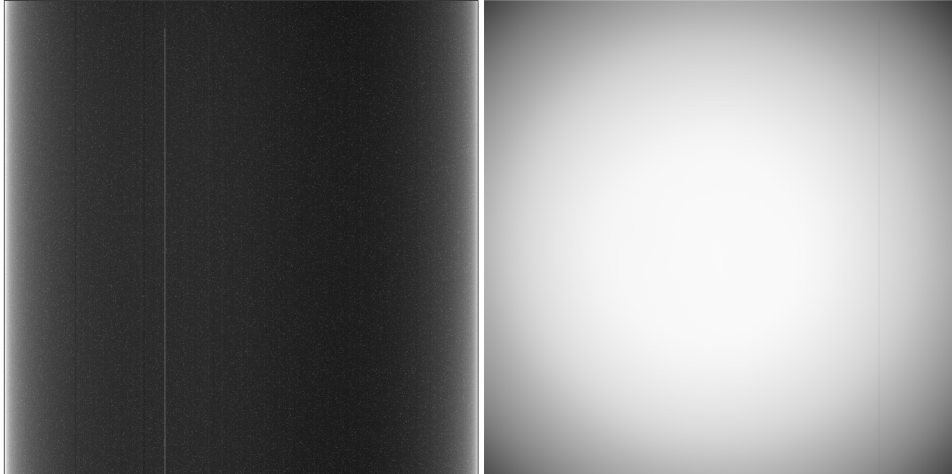


Figure 2.1: Masterdark (left) and masterflat (right) created at the observatory on Kraví hora in Brno by J. Kolář.

2.3 Photometric Filters

Using photometric filters allows incident light to pass only at a precisely defined wavelength intervals. The filters make it possible to compare photometric data from different observatories and also to find out more information about the examined cosmic objects. There are three categories into which the filters are divided according to their bandwidth: broadband, intermediate, and narrowband. The broadband filters have their passbands larger than 30 nm, passband widths of the intermediate are between 10 and 30 nm. For the narrowband filters, their passband widths are less than 10 nm. They are often made to capture one specific spectral line (e.g. [OIII], $H\alpha$).

The set of filters with well-defined passbands and sensitivities is called a photometric system. Johnson & Morgan (1953) introduced a photometric system of three broadband filters: U (with a maximum of transmissivity in 360 nm), B (440 nm), and V (545 nm). The Johnson system was gradually supplemented by additional filters towards longer wavelengths (R , I , J , K , L , M , and N). It is currently one of the most widely used systems, mainly because it is well standardized and a large number of the stars were measured using it. The disadvantage of this system is that the bands partially overlap. The overlap of the filters U and B prevents to determine the height of the Balmer discontinuity. Filters u , g , r , i , z (Fukugita et al. 1996) from Sloan Digital Sky Survey (SDSS) are better defined and they are often used for emerging photometric projects.

The intermediate $ubvy$ system (Strömberg 1956) has narrower passbands than the Johnson system (Figure 2.2). Because of this, it is better defined and pro-

vides more information about the parameters of the observed stars. In addition to those mentioned, there are many other systems. Satellites and photometric surveys usually have their own systems. There are conversion relationships between the filters. Currently, there are over 200 different photometric systems (Munari & Fiorucci 2003).

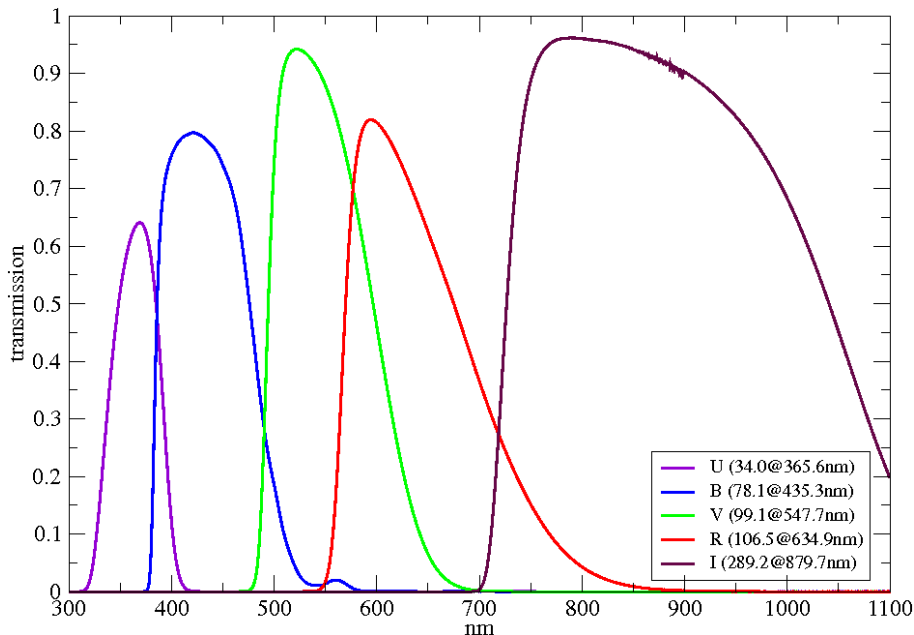


Figure 2.2: Passbands of the Johnson photometric system (Bessell 2005).

2.3.1 Colour Index

Colour index (CI) is the difference of the magnitudes m_{λ_1} and m_{λ_2} of the same object in two different photometric filters with wavelengths λ_1 and λ_2 :

$$CI = m_{\lambda_1} - m_{\lambda_2}. \quad (2.1)$$

As a general rule, λ_1 is shorter than λ_2 . The colour indices indicate some of the characteristics of the stars.

In the Johnson system, $(B - V)$ index serves as a temperature indicator (Sekiguchi & Fukugita 2000). The colour temperature T_b can be determined using this colour index. The effective temperature T_{eff} differs from the colour temperature in general. The value of the colour index and thus also the colour temperature is strongly influenced by the interstellar extinction. It causes a greater decrease in brightness in the blue area: interstellar reddening. When estimating

the temperature, the calculated value will be smaller than what is the effective temperature of the star. For better diagnostics of star properties, colour indices can be introduced as linear combinations of multiple filters in a given system. The Strömgren system uses compound indices that have only a low dependence on interstellar extinction and provide more information.

The bolometric correction BC is defined as the difference between bolometric and visual magnitude. It expresses the distribution of energy in the spectrum of an object. The bolometric correction was defined to be zero for the stars with $T_{\text{eff}} \approx 6\,800$ K. For other effective temperatures, the bolometric correction decreases in both directions. This means that the maxima of the radiated energy shift in both hot stars (towards the UV region) and cool stars (towards the IR region).

2.4 Data Analysis

2.4.1 Light Curve

The brightness of objects on the CCD images is measured using several methods. One of the most common is aperture photometry. Around the selected star an aperture of a given radius is created. The size of the aperture has to be exactly such that only the light from the star is inside. In addition to the light from the star itself, there is also background radiation inside the aperture. An annulus, in which there are no objects, is created around the aperture. The background is captured there. It is necessary to subtract the background brightness from the brightness of the star trapped in the aperture. In this way, the resulting brightness of the studied star is obtained. Aperture photometry is not mathematically demanding and in the most cases gives reliable results. This method is not suitable for dense stellar fields (e.g. globular clusters). Here, profile photometry is used, where the amount of signal is determined by interpolation with a profile function.

The comparison of brightness with another star is frequently used for obtaining information about the star under study. This is the so-called differential photometry. The result is a differential magnitude Δm :

$$\Delta m = m_v - m_{\text{comp}}, \quad (2.2)$$

where m_v and m_{comp} are magnitudes of the variable and comparison star, respectively. The comparison star should have the same or very similar distribution of the radiation spectrum as the studied star. Furthermore, it is necessary to know that the comparison star is not variable and thus its brightness

is constant. Also, the angular distance of used stars should be very small that the differences in atmospheric influences are negligible.

A graphical form of the time dependency of the star brightness is called a light curve. If the brightness of a variable star changes periodically and its period P is known a *phase curve* of the star can be constructed. Instead of the time, the *phase* φ is on the horizontal axis. The phase is minimal at the beginning of the periodic cycle, where it is 0. The maximum value of the phase is 1 and occurs at the end of the cycle. To calculate the phase, it is necessary to define the initial moment M_0 , from which the phase will be calculated. This moment is usually the time of the primary minimum. The phase is calculated as follows:

$$\varphi = \text{frac} \left(\frac{t - M_0}{P} \right), \quad (2.3)$$

where t is an observation time. The frac function ensures that the phase takes values from 0 to 1.

2.4.2 Timings of the Minima

The extremes on the light curves of the eclipsing binary stars are, among other possible phenomena, primary and secondary brightness minima. The precise knowledge of timings of the minima, including their uncertainties, is important for a determination of the period value and possible detection of the period changes. For reliable determination of the timing, it is necessary to measure the brightness of the star in a sufficiently long time scale around the minimum. In the best possible case, the entire course of the brightness changes is recorded.

There are many distinct methods for determining the timing of minimum that can generally give different results and uncertainties. The method of Kwee & Van Woerden (1956) is often used. This method assumes symmetrical light curves and sufficient coverage of the curves in parts of the brightness changes. The method also required equidistant points on the light curve. However, the use of the Kwee-van Woerden method is not suitable for asymmetric or deformed light curves. Furthermore, the uncertainties of the calculated times obtained by this method can be misleading and underestimated (Mikulášek et al. 2013).

Data from photometric surveys (e.g. ASAS, MACHO) capture the brightness of the objects on a long time scale. Frequency of the measurements is usually not enough high to cover the separate minima sufficiently. Thus, when using them, one could create a template light curve. The template curve is expressed by a suitable function e.g. harmonic polynomial or exponential function. The timing of the extremes can then be precisely and reliably determined by the phase shifts of the observed and the template light curve (Mikulášek et al. 2006).

2.4.3 $O - C$ Diagram

Major brightness changes of the eclipsing variable stars are caused by the orbital move, thus they are periodical. However, the period could not be constant. The changes can be detected by minima observations. One could obtain the observed minimum time O . From the knowledge of the orbital period P and the time of the selected basic minimum M_0 , the predicted time of the minimum can be determined. It is called the calculated time C . The difference between the time obtained from the observation and the predicted time is called $O - C$. It is usually stated in days. The time dependency of this quantity can be plotted on a graph called $O - C$ diagram. The difference is plotted on the vertical axis in the diagram. Time in Julian date or *epoch* E is plotted on the horizontal axis. The epoch expresses the number of cycles that have occurred since basic minimum M_0 . The epoch is therefore zero for this time. It is calculated similarly to the phase, but for the epoch, the integer part is taken:

$$E = \text{floor} \left(\frac{t - M_0}{P} \right). \quad (2.4)$$

The time C is then calculated using the epoch:

$$C = M_0 + PE. \quad (2.5)$$

By analysing the diagram it is feasible to refine the value of the orbital period, demonstrate its constancy or detect and correctly determine a period change. It is also possible to derive the behavior of the system or possibly a more complex structure e.g. the presence of another object in the system. Many cases of different diagram shapes and effects on them are known (Liška & Skarka 2015, Mikulášek & Zejda 2013). Below are the most common situations. Some of the instances are shown in the following figures.

- Line with zero direction, $O - C = 0$: period is constant and correctly determined, zero epoch M_0 is correct.
- Line with zero direction, $O - C \neq 0$: period is constant and correctly determined, value of M_0 is inaccurate.
- Double horizontal line: the system has a non-zero eccentricity (elliptical trajectories), the orbital period is constant.
- Oblique line: period is constant, its value is inaccurate.
- Parabola: period shortening or lengthening, caused by e.g. mass transfer.

- Sinusoidal changes in the same phase for primary and secondary minima: light-time effect (LiTE), a third body is a part of the system.
- Sine wave, primary and secondary minima are in anti-phase: apsidal motion of the system. Line of apsides changes its orientation to the observer with time, this motion is periodical.
- Sudden change of period: significant changes in the system.
- Chaotic variations: can be caused by random effects, pulsations, combinations of different variations, etc.
- Combination of multiple effects.

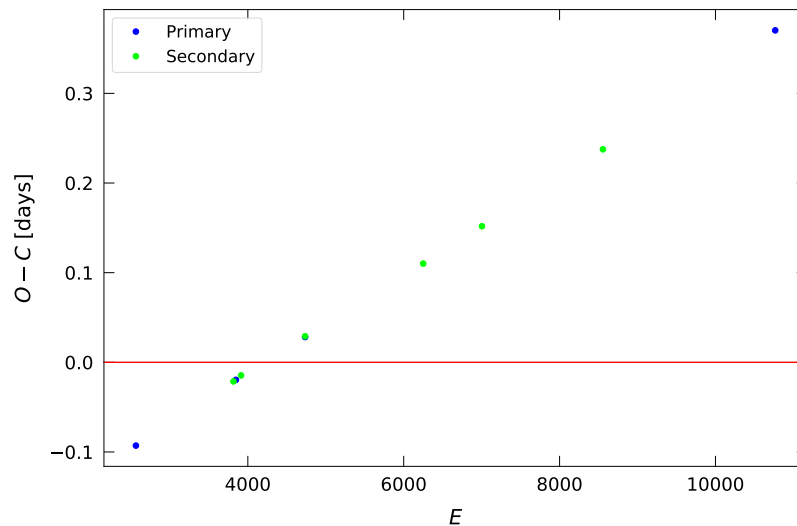


Figure 2.3: Example of $O - C$ diagram of the star (V441 And) with constant but inaccurate orbital period. The minima were taken from Lichtenknecker Database of the BAV [E1]

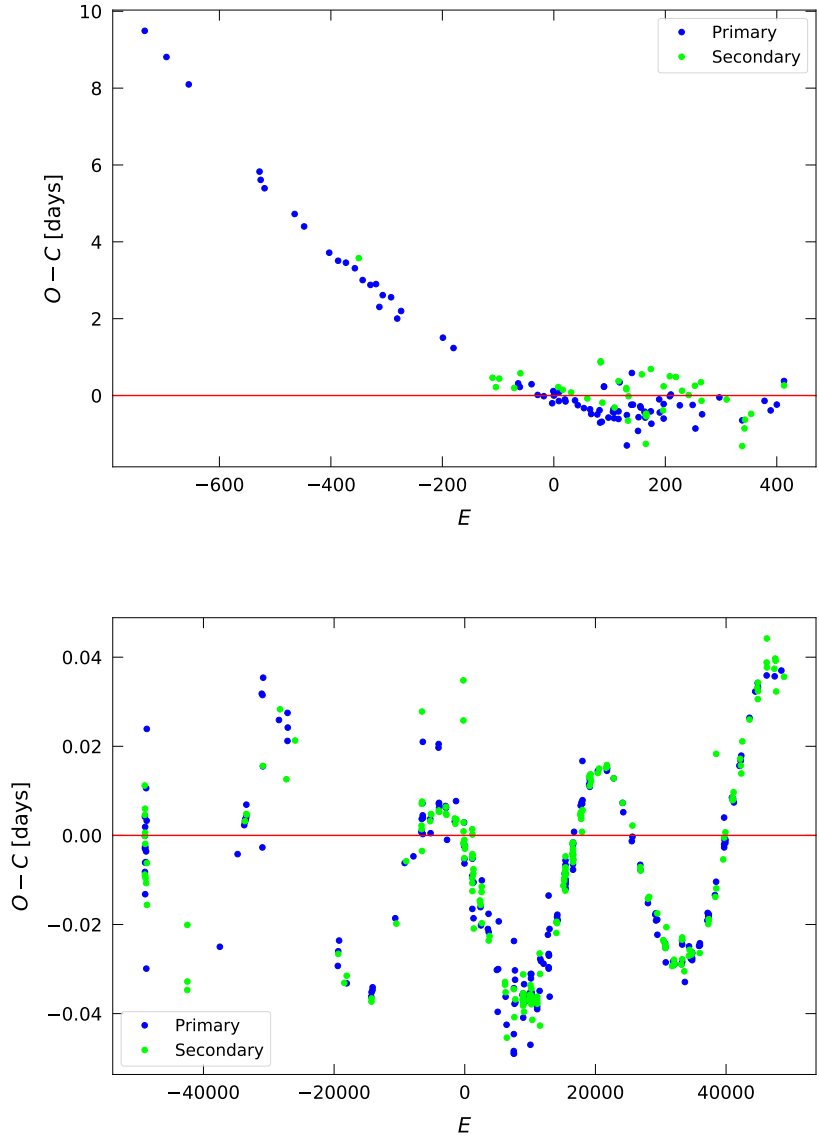


Figure 2.4: Examples of the $O-C$ diagrams, up: the period change (star RX Cas), down: LiTE (star XY Leo), from O-C Gateway [E2].

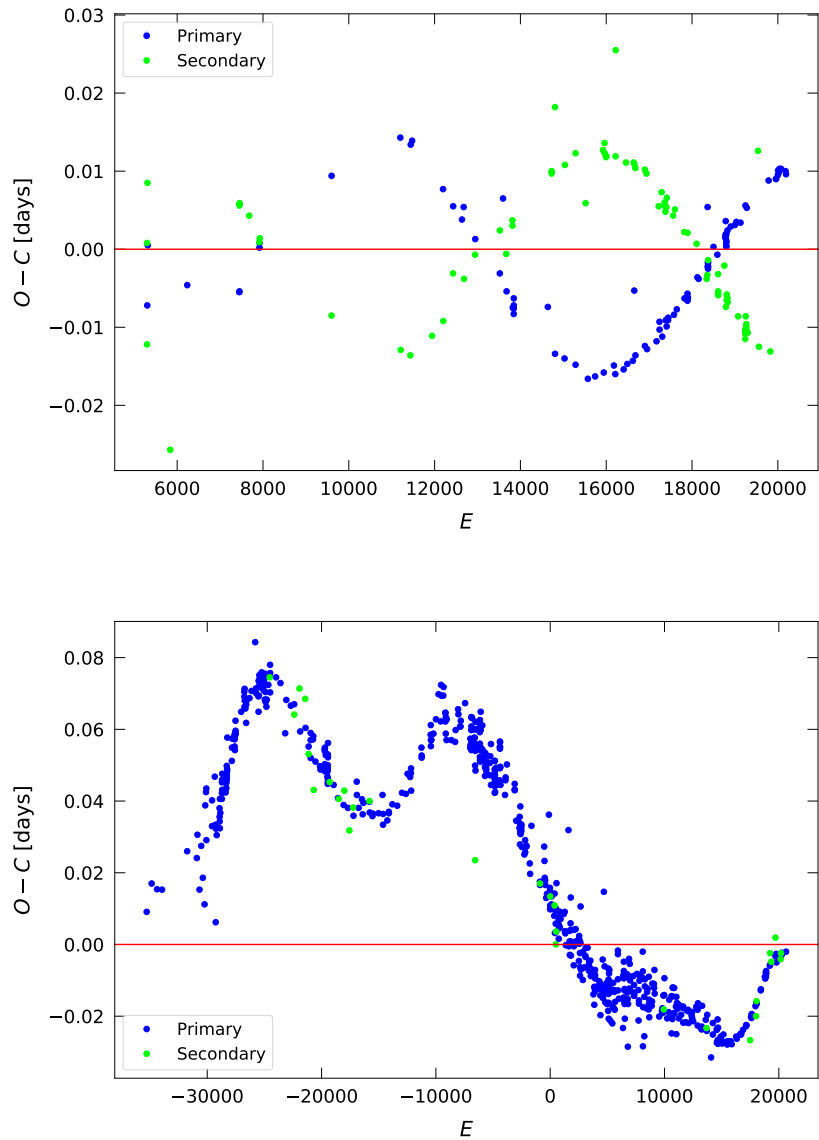


Figure 2.5: Examples of the $O - C$ diagrams, up: the apsidal motion (star CO Lac), down: combination of several effects (star RT Per), from O-C Gateway [E2].

Chapter 3

Spectroscopy

3.1 Introduction

Stellar spectroscopy deals with the formation and parameters of spectra of the stars. The spectrum means a distribution of intensity of electromagnetic radiation of the examined object depending on its wavelength λ or frequency ν . There is a clear relation between these quantities:

$$\lambda = \frac{c}{\nu}, \quad (3.1)$$

where $c = 299\,792\,458 \text{ m s}^{-1}$ is the speed of light. The electromagnetic radiation comes from the stellar photospheres. Thus, only the surface of the stars could be observed. The spectra are, typically, continuous with absorption and emission lines.

The spectral lines are not perfectly sharp. Their shape is not a δ -function, but they have some specific profiles. The line always creates a profile. A line broadening occurs due to many different processes. The intensity I of the line is measured. A relative intensity, which is related to continuum intensity I_C is usually used. The central part of the spectral line is called the core. The blue and the red wings are located around the core (see Figure 3.1). Signal overflow during measurement results in oversaturation of the lines. If the spectra are oversaturated, it leads to the objectionable wing broadening. The different degrees of saturation are shown in Figure 3.1.

3.2 Spectral Classification

The stars can be divided into classes according to the occurrence and intensity of spectral lines. The different effective temperature and chemical composition

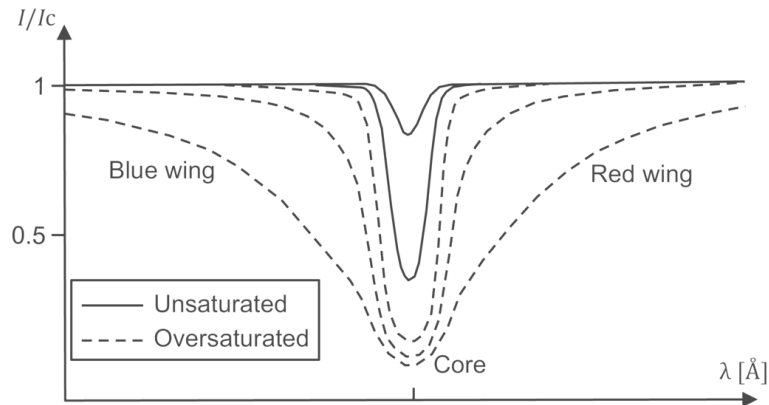


Figure 3.1: An absorption line scheme and its degrees of saturation (Trypsteen & Walker 2017).

of the photosphere of the stars is the main reason for the differences in stellar spectra. There are also other important quantities, which affect the appearance of the spectra e.g. surface gravity, rotation, magnetic field, etc.

The most common scheme is the *Harvard classification* developed at Harvard college observatory at the turn of the 19th and 20th centuries. The basis is sequence O - B - A - F - G - K - M. There are also additional classes. The stars are classified by their effective temperatures T_{eff} , with O-type stars having the highest temperatures. Furthermore, there are subclasses from 0 to 9, where 0 indicates the stars with the highest temperatures in the class.

Table 3.1: Harvard classification: spectral classes, corresponding effective temperatures, and characteristic lines (Mikulášek & Zejda 2013).

Spectral class	Effective temperature [K]	Characteristic spectral lines
O	30 000 – 50 000	He II, He I, H I, O III, C III, N III
B	11 000 – 30 000	He I, H I, C II, O II, N II, Fe III, Mg III
A	7 500 – 11 000	H I, Fe II, Ti II, V II
F	6 000 – 7 500	H I, Ca II, Ti II, Fe II
G	5 000 – 6 000	Ca II
K	3 500 – 5 000	Ca I
M	3 000 – 3 500	TiO, VO, Ca I

This classification is based on effective temperature only. However, there are also other parameters affecting the appearance of the spectra. The spectral lines have different intensities at the same temperature T_{eff} and different surface gravity g . The position of the star on the Hertzsprung-Russell (HR) diagram can be estimated using g . *Morgan-Keenan classification* (M-K) is used for a more detailed distribution of stellar spectra (Morgan & Keenan 1973). It includes effective temperature information and complements it with *luminosity classes* (Table 3.2).

Table 3.2: Luminosity classes.

Luminosity class	Name
Ia	Luminous supergiants
Ib	Supergiants
II	Bright giants
III	Giants
IV	Subgiants
V	Main-sequence stars
VI	Subdwarfs
VII	White dwarfs

3.2.1 Spectral Type B

B-type stars belongs to hot stars with effective temperatures between 11 000 K and 30 000 K. They are very bright objects with typical luminosities of hundreds and thousands of solar luminosities⁴ [E3]. The lines of neutral helium He I and neutral hydrogen H I dominate in the spectra. The hydrogen lines amplify for higher subtypes. Figure 3.2 depicts optical spectra of B-type stars on the main sequence.

3.3 Measuring

The electromagnetic radiation is decomposed to the spectrum by dispersing members, the main part of spectrograph. According to this element, there are several types of spectrographs. Historically, the prism spectrograph was mostly

⁴Solar luminosity $L_{\odot} \approx 3.828 \times 10^{26}$ W

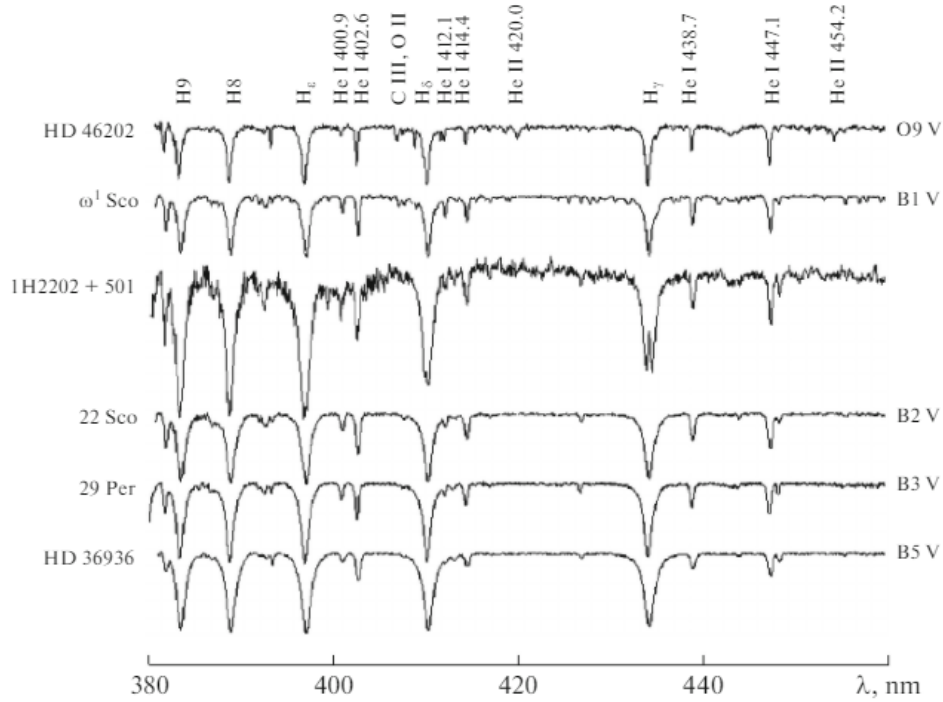


Figure 3.2: B-type stars spectra in shortwave region with their typical spectral lines (Simon et al. 2019), there is also O9 star spectrum for comparison.

used. Grating spectrographs using a diffraction grating, and echelle spectrographs are widely used. Two diffraction gratings (eventually one gratings and one prism) are parts of the echelle spectrograph. They are rotated 90 degrees relative to each other.

Photography has been used in the past to record spectra. Currently, the CCD camera is the most common detector in stellar spectroscopy. Bad pixels, blurry edges, and cosmic particles traces have to be corrected on the CCD frames before the basic data reduction. Bias, dark frame and flat field are applied during the reduction. Calibration frames for wavelength calibration are also created. Spectral lines with known wavelengths in the comparison spectrum are identified and a calibrated spectrum is obtained.

3.4 Radial Velocities

The components of binary system orbit their common centre of mass. During this movement, the stars alternately approach and also move away from the observer. As a result, their *radial velocities* are periodically changing. The star

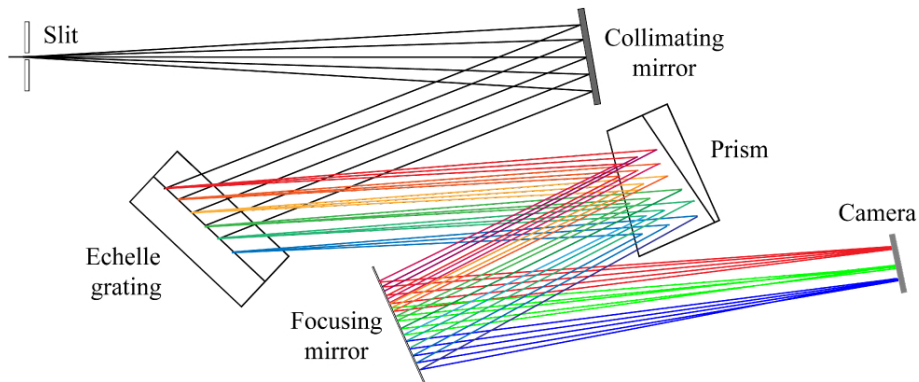


Figure 3.3: Scheme of the echelle spectrograph with gratings and prism [E4].

velocities oscillate around the radial velocity of the centre of mass. The spectral lines wavelengths shift at a non-zero radial velocity due to the Doppler effect. Measuring the line shifts, one can calculate radial velocity v_{rad} :

$$v_{\text{rad}} = c \frac{\lambda - \lambda_0}{\lambda_0}, \quad (3.2)$$

where λ is measured wavelength and λ_0 is laboratory line wavelength.

The spectral line could split in two lines during the orbital motion. In this case, radial velocities of both stars can be measured. If there both components are visible in the spectrum, these binary stars are called double-line binaries (SB2). For single-line binary (SB1) only one component can be distinguished in the spectrum.

From the long measurements, the time dependence of radial velocities can be obtained. The radial velocity curve is a graphic form of this dependency. Two sines waves in antiphase represent SB2 stars with circular trajectories (Figure 3.4). Various deformed periodic curves indicate objects with elliptical trajectories, mostly combined with different orientation towards the observer.

Analysis of the light curve and the radial velocity curve of an eclipsing binary leads to the determination of important system characteristics, which would be difficult to determine any other way. One can analyze the data and obtain absolute dimensions and masses of the components. It is possible to derive the system distance when determining the absolute magnitude and the known observed magnitude.

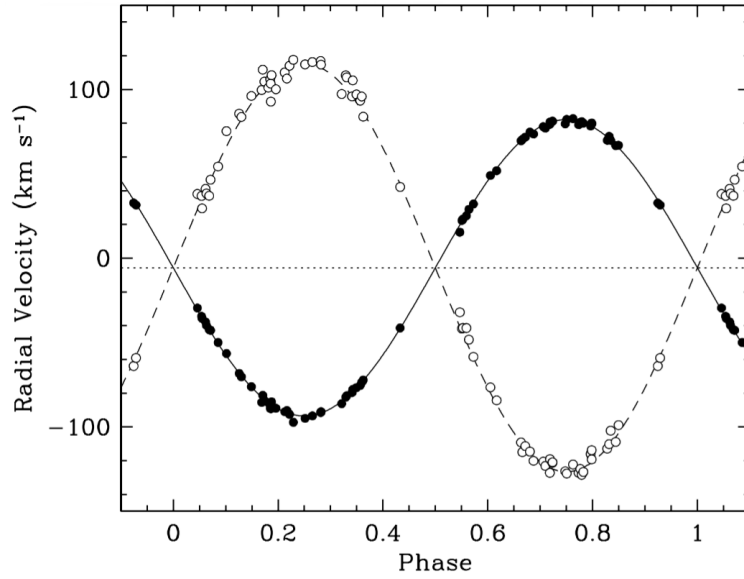


Figure 3.4: Example of radial velocity curve of binary components with circular trajectories, specifically two stars of triple system V1061 Cyg (Torres et al. 2006).

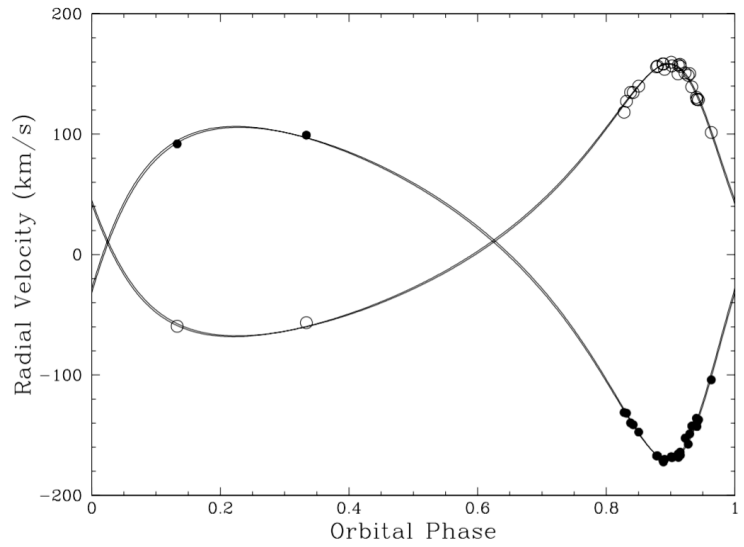


Figure 3.5: Example of radial velocity curve of eccentric binary, the components have elliptical trajectories. FT Ori binary system is shown, the system eccentricity $e = 0.409$ (Sabby et al. 2011).

Chapter 4

Selected objects

4.1 Basic Information

B-type binary stars can be studied in our Galaxy and even in nearby galaxies due to their high brightness. The Large Magellanic Cloud contains many different types of stars including binary systems. They could be used for determine the basic stellar parameters and the distance of the galaxy. Recently, a large amount of new observational data has been added, for instance from OGLE survey and the Gaia and TESS satellites. These data can significantly contribute to the analysis of eclipsing binary stars. In this study, two detached eclipsing stars in LMC and other two in the Galaxy were chosen for a research.

All the four systems are spectral type B as for the primary component. The orbital periods are around 6 days. The stars have not yet been analyzed in detail, or only the first studies has been carried out. Analysis of the spectra is mostly absent. GX Lacertae and TT Lyrae in the Galaxy and two LMC stars with the names from OGLE survey (Pawlak et al. 2016) OGLE LMC-ECL-7641 and OGLE LMC-ECL-17660 were analyzed in this work. Basic parameters of these stars are in Tables 4.1 to 4.4.

4.1.1 GX Lac

The system GX Lac (BD+56 2855; HD 240055) is a long known variable star. It was used as a comparison star to the eclipsing binary CO Lac. However, Uitterdijk (1934) found out that its brightness is changing and processed the observations from photographic plates. Kreiner (1968) introduced for the first time the light ephemeris, the depths of both minima, and the duration of the eclipses. Brightness changes are quite significant, in the order of tenths of magnitude. This star has not been properly examined although its variability is known for a long time. Only a few minima observations are available (see section 5.1). There are

other two eclipsing binaries in the GX Lac vicinity: the mentioned CO Lac and V0474 Lac. The small angular distance of these stars allows to observe them simultaneously.

Table 4.1: Information about GX Lac.

Parameter	Value	Source
Right ascension	22 ^h 46 ^m 16.78 ^s	SIMBAD [E5]
Declination	+56°51'07.74''	SIMBAD
V [mag]	10.1 – 10.4	VSX [E6]
Spectral type	B5	Cannon & Pickering (1993)
P [days]	6.3552417	Kolář (2020)
M_0 [HJD]	2 456 495.4607	Kolář (2020)

4.1.2 TT Lyr

TT Lyr (BD+41 3353; AN 136.1910) has a very significant primary minimum, whose depth varies substantially in different photometric filters. The secondary minimum, on the hand, is very weak, especially in the blue colour. Historical observations have focused mainly on the primary minima. Nijland (1913) published the first times of minima. The first effort to analyze the light curve was made by Shapley (1913). Eclipsing variable star V0461 Lyr is located at a small angular distance from TT Lyr.

Table 4.2: Information about TT Lyr.

Parameter	Value	Source
Right ascension	19 ^h 27 ^m 36.31 ^s	SIMBAD
Declination	+41°42'05.53''	SIMBAD
V [mag]	9.34 – 11.43	VSX
Spectral type	B2	Wright et al. (2003)
P [days]	5.243727	VSX
M_0 [HJD]	2 454 357.4341	Hübscher et al. (2008)

4.1.3 OGLE LMC-ECL-7641

The star OGLE LMC-ECL-7641 (BI 74) is not known as a variable for a long time. Brunet et al. (1975) include it in the catalogue of O-B2 stars in LMC. First spectral type determination was done by Conti et al. (1986*a*). Its variability was proved by OGLE survey. Zasche et al. (2020) showed the apsidal motion of this star and made the light curve analysis.

Table 4.3: Information about OGLE LMC-ECL-7641.

Parameter	Value	Source
Right ascension	05 ^h 06 ^m 51.94 ^s	SIMBAD
Declination	−68°25′46.52″	SIMBAD
V [mag]	14.027	OGLE
Spectral type	B3	Conti et al. (1986 <i>b</i>)
P [days]	6.3300107	OGLE
M_0 [HJD]	2 457 001.5851	OGLE

4.1.4 OGLE LMC-ECL-17660

OGLE LMC-ECL-17660 (TIC 391813788) is an eclipsing binary, which was observed within the OGLE and MACHO surveys (Derekas et al. 2007, Faccioli et al. 2007). The orbital period and the depths of the minima has been diagnosed. There is no detailed study of its light curve. Spectroscopic measurements to determine the spectral type are also missing.

Table 4.4: Information about OGLE LMC-ECL-17660.

Parameter	Value	Source
Right ascension	05 ^h 30 ^m 22.13 ^s	SIMBAD
Declination	−69°14′52.05″	SIMBAD
V [mag]	14.251	OGLE
Spectral type	B2 – B5	This work
P [days]	6.2290904	OGLE
M_0 [HJD]	2 457 005.0329	OGLE

4.2 Observations

4.2.1 Photometry

New photometric measurements were taken from April 2018 to May 2021. GX Lac and TT Lyr were observed at Masaryk University Observatory⁵ (MUO) in Brno using a G4-16 000 CCD camera with Johnson filters and reflecting Newton-type telescope 600/2780 mm [E7]. Dark frames were created during all observations. Flat field frames were taken if the weather conditions were suitable. Otherwise, the frames, which were taken at the nearest observation night were used.

The LMC stars were observed using the Danish telescope (DK154) at La Silla in Chile [E8]. The CCD E2V CCD 231-41 with Bessel photometric filters was used for the measurements. These observations were carried out from December 2020 to February 2021. The telescope was controlled remotely from the Czech Republic. The observation campaign was organized by J. Kolář for these stars. M. Zejda and R. F. Auer were participated in the campaign. A total number of 17 own observations of GX Lac, 3 of TT Lyr, 4 of OGLE LMC-ECL-7641 and 1 of OGLE-17660 were performed. The high number of GX Lac observations is due to a longer study of this star. Information about the observations is summarized in Table 4.5.

Table 4.5: Journal of the new own photometric observations.

Star	Date	Device	Filters
GX Lac	30/04/2018	Newton 600/2780	BVR
GX Lac	07/05/2018	Newton 600/2780	BVR
GX Lac	30/05/2018	Newton 600/2780	BVR
GX Lac	19/07/2018	Newton 600/2780	BVR
GX Lac	05/09/2018	Newton 600/2780	BVR
GX Lac	08/09/2018	Newton 600/2780	BVR
GX Lac	11/09/2018	Newton 600/2780	BVR
GX Lac	12/09/2018	Newton 600/2780	BVR

⁵16°35'00."16 E, 49 ° 120'16".20 N, elevation: 305 m

Table 4.5 (continued)

Star	Date	Device	Filters
GX Lac	27/09/2018	Newton 600/2780	BVR
GX Lac	16/10/2018	Newton 600/2780	BVR
GX Lac	17/10/2018	Newton 600/2780	BVR
GX Lac	24/10/2018	Newton 600/2780	B
GX Lac	31/10/2018	Newton 600/2780	B
GX Lac	29/10/2019	Newton 600/2780	BVR
GX Lac	14/11/2019	Newton 600/2780	BVR
GX Lac	24/11/2019	Newton 600/2780	VR
GX Lac	30/11/2019	Newton 600/2780	BVR
TT Lyr	20/07/2020	Newton 600/2780	BVRI
TT Lyr	27/07/2020	Newton 600/2780	BVRI
TT Lyr	25/08/2020	Newton 600/2780	BVRI
OGLE LMC-ECL-7641	27/12/2020	DK154	BVR
OGLE LMC-ECL-7641	30/12/2020	DK154	BVR
OGLE LMC-ECL-7641	31/01/2021	DK154	BVR
OGLE LMC-ECL-7641	03/02/2021	DK154	BVR
OGLE LMC- ECL-17660	17/01/2021	DK154	BVR

The frames were reduced and processed by standard reduction procedure using C-Munipack⁶ software. Master dark and master flat were applied. Com-

⁶c-munipack.sourceforge.net/

parison and check stars were chosen in a such way that the angular distance to the variable star is small and the spectral type is similar to the variable star. Other available data were collected from several photometric surveys and observers (Table 4.6). These data were combined with the own observations to construct the light curves.

4.2.2 Spectroscopy

Spectroscopic measurements of GX Lac were carried out in Ondřejov by Perek 2m Telescope [E9] by staff members of the Stellar Physics Department of the Astronomical Institute of the Czech Academy of Sciences (ASU) upon request. Data for other examined objects were adopted from ESO UVES spectrograph [E10] and LAMOST survey DR4 [E11] and DR5 [E12]. Spectra were already reduced and prepared for the analysis. The spectral line wavelengths determination was done in SPLAT-VO [E13]. Further information about spectral types and radial velocities of the stars were obtained from available literature (details in sections 4.1 and 5.4).

Table 4.6: Journal of observations.

Star	Observer	Observatory	Filters	Time interval
GX Lac	Auer R.	SMO ⁷	BVRI	July 2013 – July 2015
GX Lac	Zejda M.	MUO	BVRI	June 2010 – August 2018
GX Lac	Samolyk G.	AAVSO [E6]	V	September 2012 – December 2020
GX Lac	TESS	TESS	TESS	September 2019 – November 2019
TT Lyr	Auer R.	SMO, TRO ⁸	BVRI	July 2020 – September 2020
TT Lyr	Zejda M.	MUO	BVRI	May 2021
TT Lyr	Urbaník M.	Kysucká hvězdáreň	Clear	May 2016
TT Lyr	Itoh. H.	Tokyo, Japan	V	August 2020
TT Lyr	Cook S.	AAVSO [E6]	V	August 2020
TT Lyr	TESS	TESS	TESS	July 2019 – August 2019

Table 4.6 (continued)

Star	Observer	Observatory	Filters	Time interval
OGLE LMC-ECL-7641	OGLE III	Las Campanas	VI	September 2001 – May 2009
OGLE LMC-ECL-7641	OGLE IV	Las Campanas	VI	March 2010 – March 2014
OGLE LMC-ECL-7641	MACHO	Mt. Stromlo	BR	July 1992 – January 2000
OGLE LMC-ECL-7641	DK154	La Silla	BVRI	October 2013 – December 2020
OGLE LMC-ECL-17660	OGLE III	Las Campanas	VI	November 2001 – March 2009
OGLE LMC-ECL-17660	OGLE IV	Las Campanas	VI	March 2010 – March 2014
OGLE LMC-ECL-17660	MACHO	Mt. Stromlo	BR	July 1992 – January 2000
OGLE LMC-ECL-17660	DK154	La Silla	VRI	November 2012 – February 2020

Table 4.7: Spectroscopic observations from which radial velocities were determined.

Star	Observer	Observatory	Date
GX Lac	Dvořáková, Kortusová	Ondřejov	23/03/2020
GX Lac	Skarka, Kortusová	Ondřejov	06/11/2020
GX Lac	Blažek, Řezba	Ondřejov	21/11/2020
GX Lac	Blažek, Sloup	Ondřejov	02/12/2020
GX Lac	Kabáth, Novotný	Ondřejov	04/12/2020
GX Lac	Raine, Krejcar	Ondřejov	29/12/2020

⁷South Moravian Observatory⁸Toscana Remote Observatory

Table 4.7 (continued)

Star	Observer	Observatory	Date
OGLE LMC-ECL-7641	ESO	ESO-VLT-U2, UVES	03/10/2018
OGLE LMC-ECL-7641	ESO	ESO-VLT-U2, UVES	08/10/2018
OGLE LMC-ECL-7641	ESO	ESO-VLT-U2, UVES	04/11/2018
OGLE LMC-ECL-7641	ESO	ESO-VLT-U2, UVES	26/11/2017
OGLE LMC-ECL-7641	ESO	ESO-VLT-U2, UVES	13/12/2017
OGLE LMC-ECL-7641	ESO	ESO-VLT-U2, UVES	05/12/2016
OGLE LMC-ECL-7641	ESO	ESO-VLT-U2, UVES	06/12/2016
OGLE LMC-ECL-7641	ESO	ESO-VLT-U2, UVES	06/12/2016
OGLE LMC-ECL-17660	ESO	ESO-VLT-U2, UVES	19/10/2018
OGLE LMC-ECL-17660	ESO	ESO-VLT-U2, UVES	01/11/2018
OGLE LMC-ECL-17660	ESO	ESO-VLT-U2, UVES	13/12/2017
OGLE LMC-ECL-17660	ESO	ESO-VLT-U2, UVES	06/12/2016
OGLE LMC-ECL-17660	ESO	ESO-VLT-U2, UVES	06/12/2016
OGLE LMC-ECL-17660	ESO	ESO-VLT-U2, UVES	07/12/2016
OGLE LMC-ECL-17660	ESO	ESO-VLT-U2, UVES	07/12/2016

Chapter 5

Data Analysis

5.1 Period Analysis

New photometric observations also recorded several new minima of brightness. The minima timings and their uncertainties were calculated in the AMPER database [E14] and by SILICUPS software [E15]. The light curve profile in SILICUPS and AMPER is described by model function. The phenomenological model was suggested by Mikulášek (2015).

Available minima timings from databases O-C Gateway [E2] and Lichtennecker Database of the BAV [E1] were combined with new minima from the observations. Used minima timings for all stars are summarized in Appendices. Most of the calculated times have not any given uncertainties, or their uncertainties are very unclear. For these reasons, the individual measurements to given minima timings were sought. However, not all data could be traced.

$O-C$ diagram was constructed for each binary system with the knowledge of the orbital period P and the time M_0 . Since not all individual measurements are available and for some data the values of uncertainties are not realistic (more in individual cases), the iterative procedure described in Mikulášek & Zejda (2013) was chosen for the diagram analysis.

In the beginning, all points have the same uncertainty. Period constancy, its determination accuracy, and eventually period change is determined from the diagram shape. Subsequently, the fit with a suitable function that corresponds to the given phenomenon was performed. Standard deviations ΔT were obtained as a result of the difference between the model function and the measurements.

After this step, the data were divided into n groups. Every group contains at least five points. The data were sorted according to common observational parameters, mostly by a detector. The standard deviation of ΔT values was

done for each group. This quantity σ_n is taken as a new value of uncertainty in every group. New fitting will be calculated with these uncertainties and new values of ΔT were obtained. The procedure is repeated until the uncertainties σ_n stop changing. The model function and more accurate period value can be obtained at the end of this iterative process.

GX Lac

There is only a small amount of available GX Lac minima. Some measurements could not be used for period analysis. The timing from Uitterdijk (1934) is based on a light curve, which consists of only four points on the descending branch of the eclipse. The time of the point with the highest brightness decrease is considered as a minimum. The brightness decrease is 0.24 mag at this time. However, the brightness change of the primary minimum is about 0.30 mag, therefore, the actual minimum was not observed. For this reason, this time was not included in the analysis. Häussler (1980) published only the times of extremes on the light curve. However, it is not a measurement of a single object, but a long-term systematic observation of a part of the sky. A normal point of this light curve is based on approximately one month monitoring. Therefore, the measurements did not have to capture the minimum. The $O - C$ values differ significantly from other observations. Therefore, this data could not be used.

The visual minimum obtained by Cook (Samolyk 2013) has no uncertainty and further information about the observation. This observation does not fit with others and was not used. Two minima from Samolyk (AAVSO) were calculated in AMPER. It was necessary to exclude one minimum from Samolyk (2019) because of the suspicious light curve shape. Minimum calculated by Urbaník (Hoňková et al. 2013), Dienstbier, and Šmelcer were adopted from O-C Gateway. The calculations were made in [E16] by bootstrapping.

TESS data contributed significantly to the analysis. The observations cover the entire course of brightness changes and capture four primary and eight secondary minima. The minima times were calculated in SILICUPS software. A complete list of minima timings and additional information is in Appendices (Table A.1).

The $O - C$ diagram was constructed. The HJD time 2 456 495.4607 from Auer's observation was selected as a M_0 moment. The initial orbital period $P = 6.3552417$ days was obtained from Kolář (2020). The $O - C$ values displayed in Figure 5.1 are based on this ephemeris. There are no error bars because not all errors were known. Primary and secondary minima are shifted vertically relative to each other. This shape indicates that the components of the system have elliptical trajectories. The period seems to be constant.

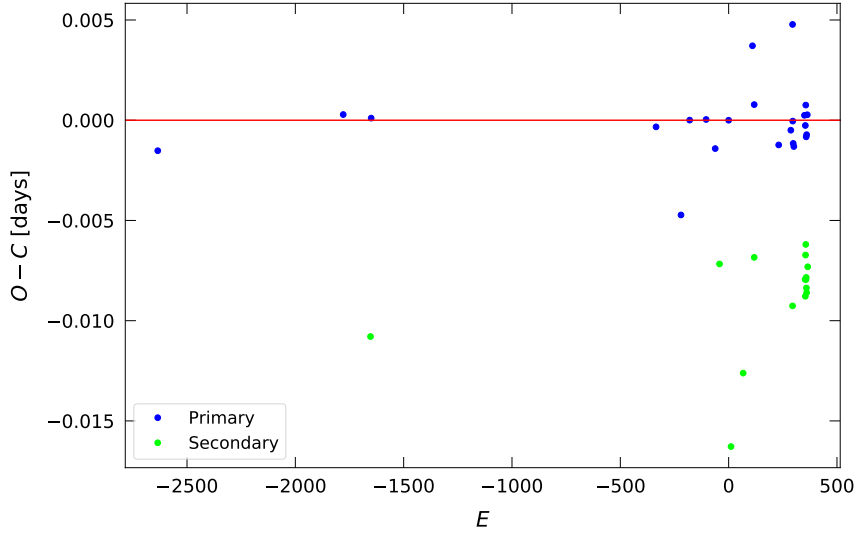


Figure 5.1: $O - C$ diagram of GX Lac.

Primary and secondary minima were fitted by a straight line $y = ax + b$ according to the above described procedure. Both data sets (primary and secondary minima) were divided into two groups: ground based CCD and photoelectric measurements, and TESS observations. After four iterations, the parameters of the line were obtained, which did not change. The parameters were $a = 3.75 \pm 0.10 \times 10^{-7}$ days and $b = -4.0 \pm 4.0 \times 10^{-5}$ days for primary minima and $a = 2.0 \pm 1.0 \times 10^{-6}$ days and $b = -9.0 \pm 9.0 \times 10^{-3}$ days for secondary minima. Ephemeris was corrected for the coefficients found by iterating the primary minima because they contain more points and were more reliable. New orbital period is $P = 6.355242075 \pm 0.000000010$ days and $M_0 = 2\,456\,495.46066 \pm 0.00004$ (HJD). Figure 5.2 depicts the $O - C$ diagram of GX Lac with these new values. Each minimum has its error calculated at the end of the iteration process.

TT Lyr

A large number of minima observations of TT Lyr is known. Most of the measurements were visual or photographic. Some observations and publications about them were not found. The observations done by Harwood (Shapley 1917, Harwood & Shapley 1933) have a large variance of $O - C$ values. Nijland (1913) observed Algol-type eclipsing binaries including TT Lyr. Minima times from original publication differ from times in O-C Gateway. A secondary minimum

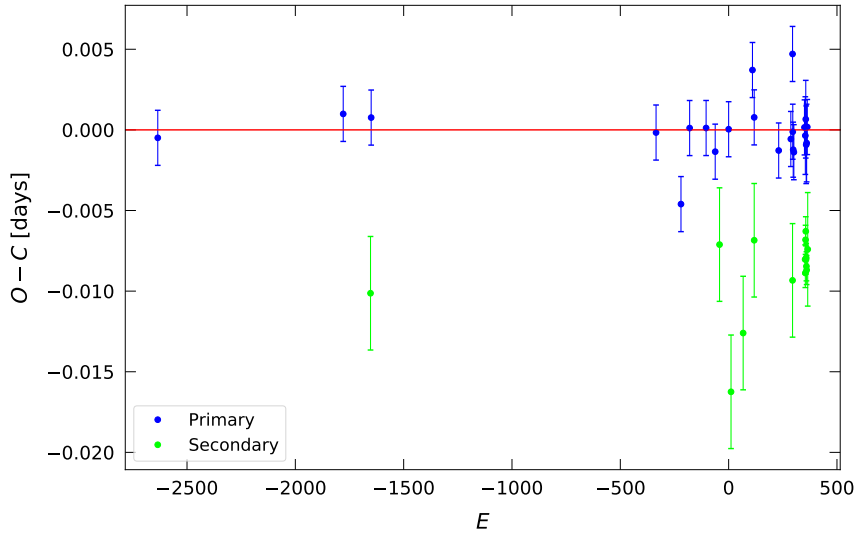


Figure 5.2: New $O - C$ diagram of GX Lac with calculated uncertainties.

from Gaposhkin was not used because it was significantly apart from other observations.

Lause (1936, 1938) gives time in JD. However, O-C Gateway shows these times as they are in HJD. It was therefore necessary to take the original times and calculate HJD. Each minimum has its weight from 0 to 4. The minima, which are based only on few light curve points or where the points are on a descending or ascending branch was not taken into account (their weight was zero). However, the uncertainties are not stated.

Ahnert (1949) summarized the measurements of Ahnert and Pohl. There are eleven primary minima from photographic plates. The publication contains magnitudes in the determined times. The magnitude values do not correspond to the expected value of brightness change. The $O - C$ values from the databases vary significantly and confirm that there are no minima times captured. Therefore, this data was not plotted on the diagram and used.

The minima times from the TESS satellite were calculated by SILICUPS software. Further observations were taken from Urbaník [E2], Auer, and Itoh [E17]. Moreover, new observations made at MUO were added. AMPER database was used for calculation the minima times. Almost all used minima were primary and there were only a few observations with secondary minima. The very small brightness change is probably the main reason for the small number of observations of

secondary minima. The minima and information about them are in Appendices (Table A.2).

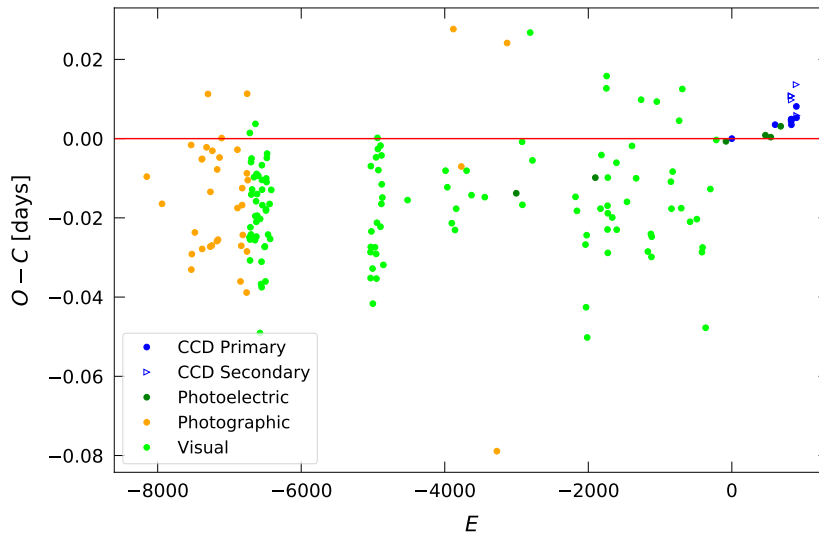


Figure 5.3: $O - C$ diagram of TT Lyr.

Orbital period of TT Lyr was adopted from VSX database: $P = 5.243727$ days. The time $M_0 = 2\,454\,357.4341$ (HJD) was obtained from the CCD observation of Jungbluth (Hübscher et al. 2008) and used for construction of the $O - C$ diagram (see Figure 5.3). Most of the visual and photographic data are vertically shifted below 0. It is not clear whether the period varied or was constant from the large variance of $O - C$ values. The visual observers could be affected by inaccurate ephemeris. The similar situation was proved in Zhu et al. (2012) for BS Vul system. The observations on the photographic plates could be only magnitude decrease on the light curve and not precisely the minima. The minimum long duration can also contribute to the variance of $O - C$ values, especially for visual observations. These aspects could affect minimum time determination. CCD and photoelectric observations indicate that the period is inaccurate and was fitted with an oblique line.

Primary minima were used for iteration. Some secondary minima were slightly vertically shifted and thus it was not appropriate to use them. The vertical shift could indicate an elliptical trajectory of the components, which is very close to a circle. However, there is not enough data to confirm this possibility. The minima were grouped into CCD and photoelectric ones. Seven iterations were done and the linear parameters were obtained: $a = 5.26 \pm 0.40 \times 10^{-6}$ days and

$b = 4.0 \pm 4.0 \times 10^{-4}$ days. The new value of ephemeris of TT Lyr is $P = 5.243732 \pm 0.000004$ days and $M_0 = 2454357.4345 \pm 0.0004$ (HJD). New $O - C$ diagram was constructed with calculated ephemeris (Figure 5.4). The $O - C$ values are around 0 for new minima (CCD and photoelectric) and indicate that the present orbital period is probably correctly determined within the error.

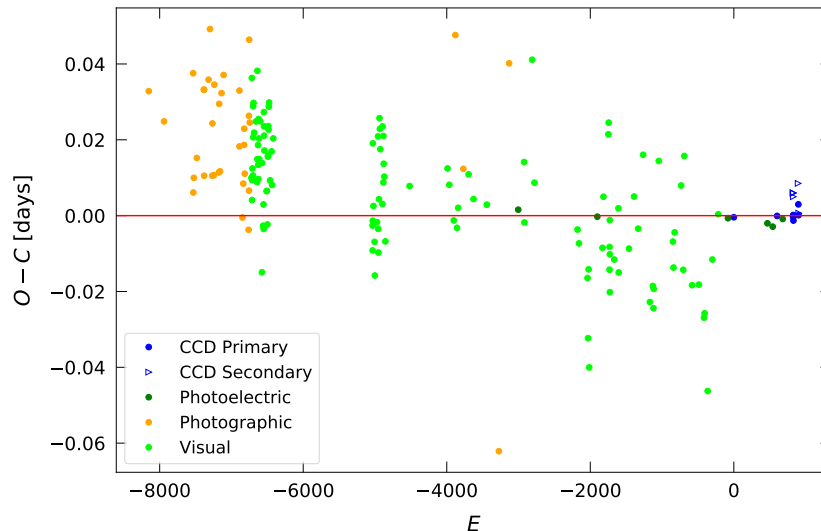


Figure 5.4: New $O - C$ diagram of TT Lyr.

OGLE LMC-ECL-7641

Data of LMC stars are contained mainly in photometric surveys. Photometric observations were made remotely using the DK154 telescope in Chile. Four observations were made to capture the eclipses. Previous observations from DK154 telescope and OGLE and MACHO surveys were adopted. Six primary and two secondary minima were captured by direct observations of the minima. This number is not sufficient for confirmation of possible period change or other effects. The light curve of OGLE LMC-ECL-7641 (Figure 5.9) shows that there are time-dependent changes of the phase of primary and secondary minimum. Zasche et al. (2020) state that this star shows an apsidal motion with a period of about 200 years with an uncertainty of about 50 years.

Data from photometric surveys were used to obtain more points in the $O - C$ diagram. Also, the data from the DASCH project [E18] were used for this analysis. These measurements are significantly older than other available observations.

First, it was necessary to construct a phase light curve (Figure 5.9) from the known ephemeris. Orbital period $P = 6.3300107$ days from OGLE and the time $M_0 = 2\,456\,963.6352$ (HJD) from La Silla observation of Zejda were used. The points on the phase light curve, which are in the minimum, were chosen. Their values of phase and observation time in HJD were found. The difference of these phases from values 1 for primary and 0.5 for secondary minima was done. The phase difference shows how these minima differ from the expected phases if the period was constant. Multiplying the phase difference by the period one could obtain the time difference. This time difference can be plotted in the $O - C$ diagram. The time of the points can be converted to epoch using ephemeris. This method gives more points in the diagram.

Figure 5.5 depicts this $O - C$ diagram with all obtained points. The minima are in antiphase, there is an apsidal motion. A point of intersection of the curves occurs around the epoch value -250 . The period of apsidal motion cannot be precisely and unequivocally determined. The time covered by the data is too short to determine the period of this phenomenon. However, it is possible at least to estimate the shortest possible period of apsidal motion. If sine wave extremes occurred in the places, where are the oldest available data, the apsidal motion period would be at least about 300 years. However, it is possible that this period could be significantly longer. From the known data the apsidal motion period determination would not be consistent. It would be necessary to have a reliable and accurate model to determine more accurate ephemeris.

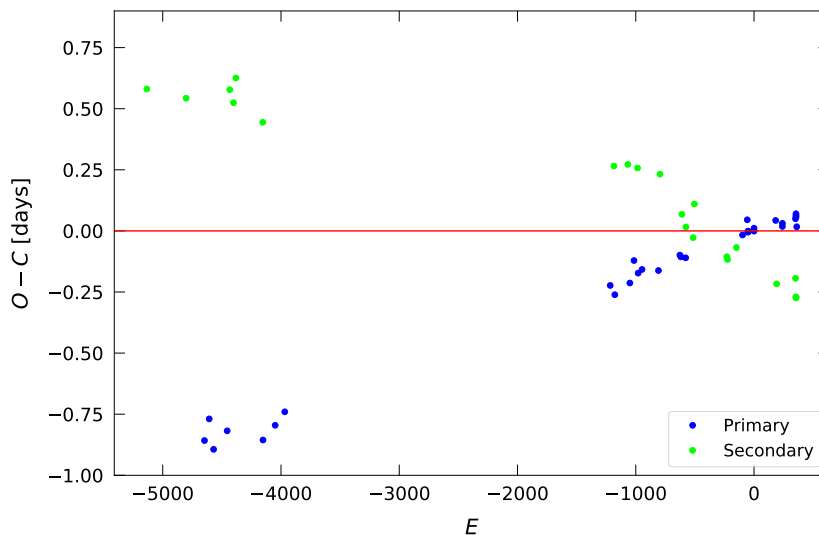


Figure 5.5: $O - C$ diagram of OGLE LMC-ECL-7641.

OGLE LMC-ECL-17660

One secondary and two primary minima of OGLE LMC-ECL-17660 were obtained from previous DK154 observations. One new own secondary minimum observation was made. This small number of points on the $O - C$ diagram cannot indicate the behavior of the system and its orbital period constancy. Other points were added using the method described above. Data from OGLE, MA-CHO, and DASCH were used here.

$O - C$ diagram (Figure 5.6) indicates that there is an apsidal motion for this star. Most of the points are found after the intersection of two sine waves. It is unclear whether the curves are at an extreme for the latest data or are still before it. Estimation of the period of apsidal motion would be very inaccurate and inconsistent. However, it can be assumed that the period is longer than 200 years.

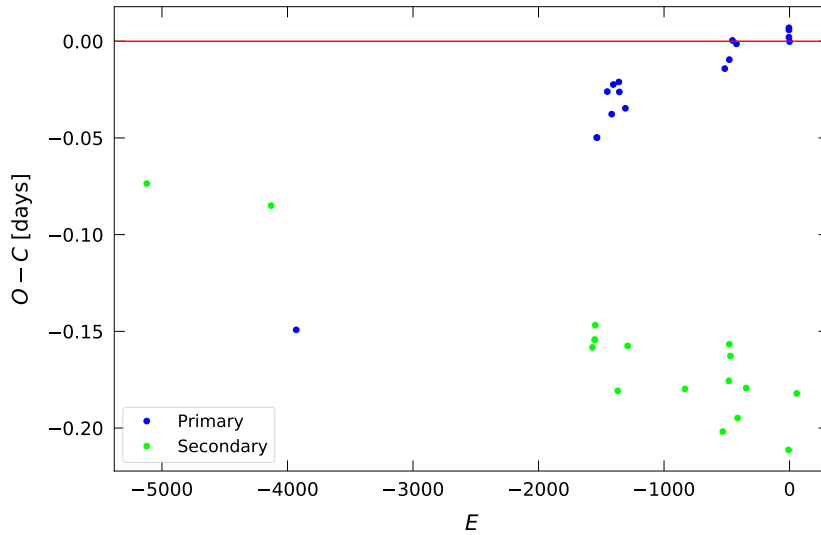


Figure 5.6: $O - C$ diagram of OGLE LMC-ECL-17660.

5.2 Light Curves

Phase light curves were constructed after period analysis and possible correction of ephemeris. TESS data were obtained using LcTools software (Schmitt et al. 2019) if they were available. Other data were obtained using Lightkurve python package [E19]. The magnitude was calibrated to 0 for the maximum flux.

The light curves are plotted in the following figures. Some data from filters had to be vertically shifted to avoid overlapping the curves to be well visible.

GX Lac

Primary and secondary minima are clearly visible on the light curve of GX Lac. Brightness decrease is similar for all used photometric filters. Primary minimum depth is about 0.30 mag for all used filters. Magnitude change for secondary minimum is about 0.15 mag. The magnitude does not change outside the eclipses.

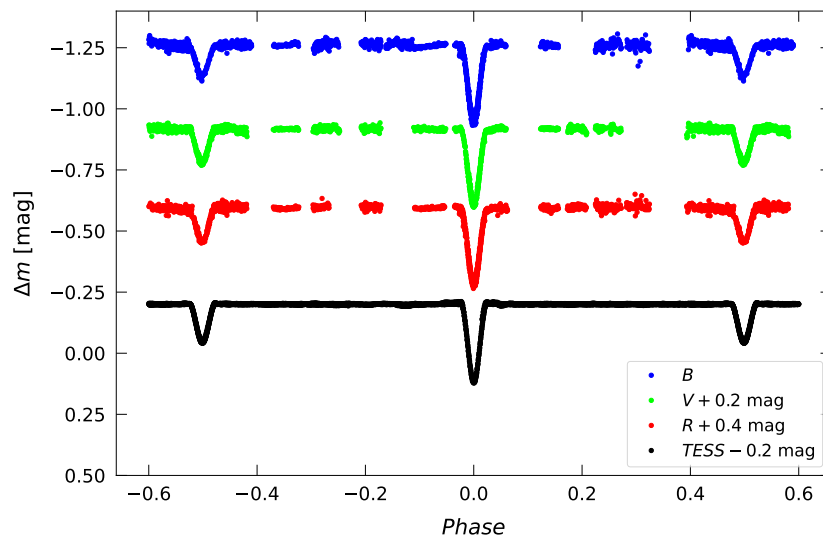


Figure 5.7: Phase light curve of GX Lac.

TT Lyr

TT Lyr system has a very deep primary minimum. The brightness decreases the most in B filter (about 2.55 mag). The decrease gradually weakens to longer wavelengths. The secondary minimum, however, is barely noticeable in the B filter and towards the red waveband is getting deeper. The largest decrease of the secondary minimum is about 0.13 mag. Brightness changes in the phases between the eclipses. Brightness slightly grows after the primary minimum. These changes are not very significant.

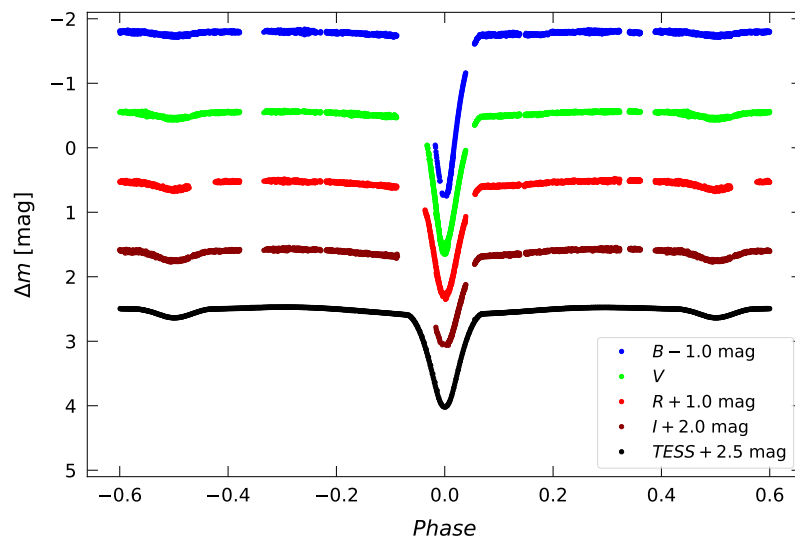


Figure 5.8: Phase light curve of TT Lyr.

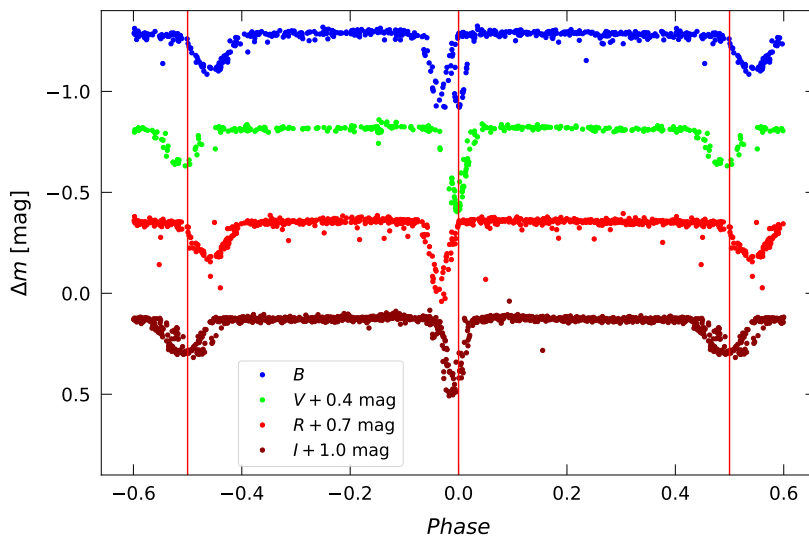


Figure 5.9: Phase light curve of OGLE LMC-ECL-7641.

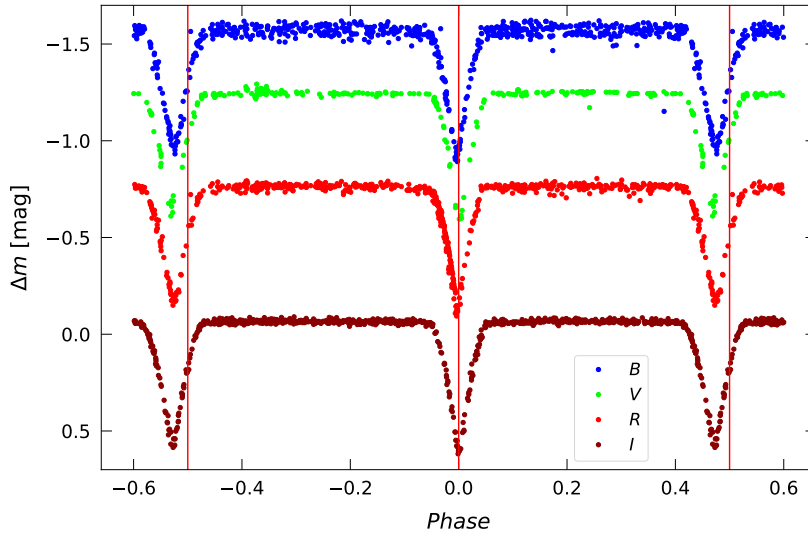


Figure 5.10: Phase light curve of OGLE LMC-ECL-17660.

OGLE LMC-ECL-7641

Both minima types are well visible on the phase light curve of OGLE LMC-ECL-7641. Their depths are about 0.4 mag for the primary and 0.2 mag for the secondary. The brightness outside the eclipses does not change essentially. The primary minimum is narrower than the secondary. The apsidal motion affects the position of both minima, which shift over time.

OGLE LMC-ECL-17660

For star OGLE LMC-ECL-17660, both minima are almost equally deep (about 0.75 mag in all colours). The position of the minima changes slightly over time, as with the previous binary system, due to apsidal motion. The magnitude is the same for the phases outside the eclipses.

5.3 Radial Velocities

The radial velocity curves are shown in the following figures. All used calculated radial velocities have uncertainties. The uncertainties for adopted data are plotted if they have been found.

GX Lac

There are six spectroscopic measurements of GX Lac. The spectra were taken by Perek 2m telescope at Astronomical Institute in Ondřejov. Only one star (primary) is detectable in the spectra. Hydrogen lines were dominated in the spectrum and were very broadened. Determining the radial velocity was thus very difficult and inaccurate. The resulting measured values reached uncertainties of up to about 30 km s^{-1} (see Figure 5.11).

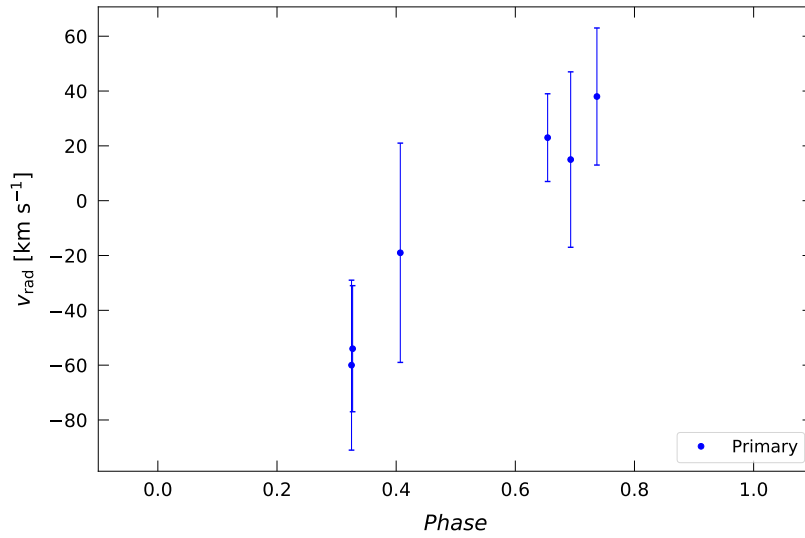


Figure 5.11: Radial velocity curve of GX Lac, only primary component was visible in the spectra. The uncertainties are very high because of lines broadening.

TT Lyr

IR spectra from APOGEE DR16 [E20] are known for TT Lyr. The radial velocities of the secondary component were adopted from there. The uncertainties of these measurements were unknown. Three values of the radial velocities were adopted from LAMOST DR4 and DR5. Figure 5.12 depicts the radial velocity curve of TT Lyr.

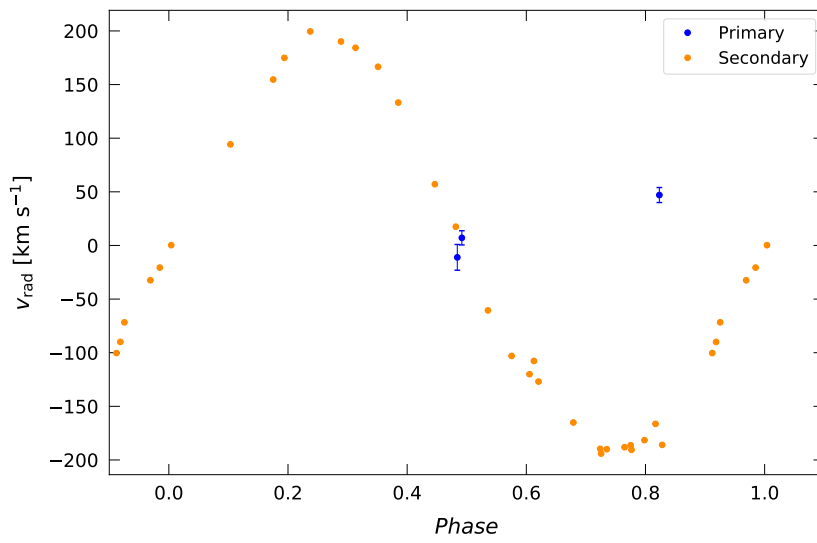


Figure 5.12: Radial velocity curve of TT Lyr. The uncertainties of the secondary component are not known.

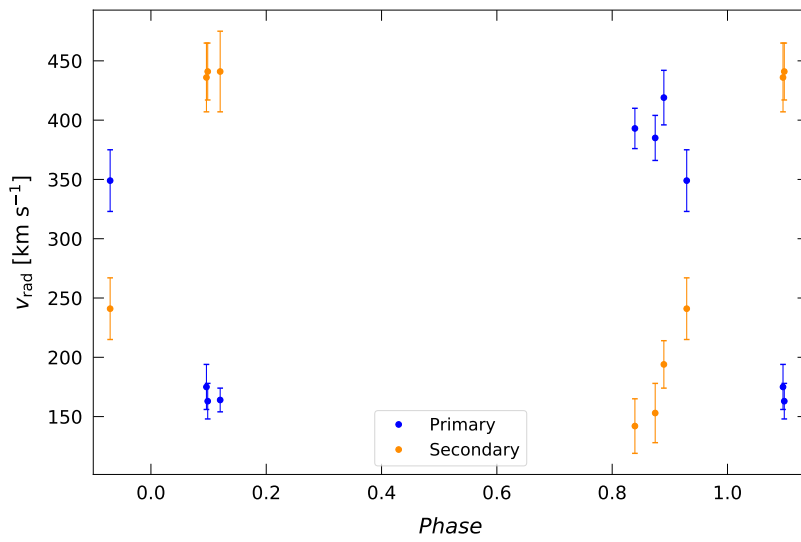


Figure 5.13: Radial velocity curve of OGLE LMC-ECL-7641.

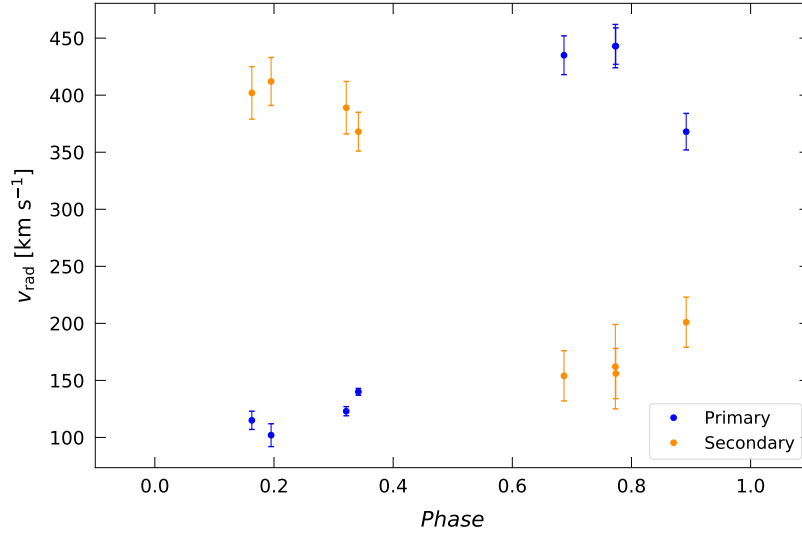


Figure 5.14: Radial velocity curve of OGLE LMC-ECL-17660.

OGLE LMC-ECL-7641

There were seven spectra of OGLE LMC-ECL-7641 available. Both components of the binary system were visible in the spectra. The radial velocity curve (Figure 5.13) indicates that the system has non-zero eccentricity, which is consistent with period analysis of this star.

OGLE LMC-ECL-17660

Both components were visible in the spectra of OGLE LMC-ECL-17660. Hydrogen and helium lines were used for wavelength determination. The radial velocity curve covers well the velocity amplitude regions. The curve shape indicates that the secondary component is probably more massive than the primary. Eccentricity value of the system is probably not very high (see Figure 5.14).

5.4 Modelling

The light curves and the radial velocity curves were constructed for all examined binary stars. The data were used to modelling the curves to obtain absolute parameters and calculate the distance. The analysis was done with PHOEBE 1 software version 0.32 (Prša & Zwitter 2005). This software is based on WD code (Wilson & Devinney 1971). The data files are inserted into the software: light

curves in different colours and radial velocities of the components. For each data set, its weight can be determined using the sigma parameter.

In the beginning, it is necessary to enter the input parameters. These parameters are usually known from the previous research or they are estimated based on tables or approximations. Some quantities are not changed. Ephemeris is typically known and fixed during the modelling. Individual parameters are calculated iteratively. It is not possible to calculate all quantities at once, as they would interfere with each other in the calculation and the results could be incorrect and skewed. A correlation matrix is part of the software. It shows how the parameters influence each other and which parameters can be calculated together. Synthetic curves are interleaved with the measured data and compared with them. Iterations are performed until the calculation error is as small as possible. However, it is necessary to pay attention to the model consistency. The quantities have to correspond to the physical reality.

It was necessary to determine the initial parameters that will enter into the model for all studied stars. The effective temperature of the primary component T_1 was estimated from known spectral type using table [E3]. Since the temperature determination was not completely accurate, the uncertainty was estimated at 500 K for all systems. Effective temperatures of the secondary components T_2 have the same values of uncertainties. Ephemeris was taken from the period analysis. Mass ratio $q = M_2/M_1$ and velocity of the centre of mass v_{cent} could be determined from the radial velocity curves first. Then the other parameters were fitted until the final model was created.

After the modelling the final parameters were used for further calculations. Luminosity L in solar luminosities could be calculated from the radius R and effective temperature T (in solar units):

$$L = R^2 T^4. \quad (5.1)$$

The observed magnitudes in filter V are known for all stars. Absolute V magnitude M_V was calculated by the following relation:

$$M_V = 4.77 - 2.5 \log L. \quad (5.2)$$

Distance modulus $m - M$ is obtained from the knowledge of observed and absolute magnitude. Subsequently, the distance d can be calculated:

$$m - M = -5 + 5 \log d. \quad (5.3)$$

However, the value calculated in this way is burdened by interstellar extinction A_V . The calculated distance without considering the extinction will be significantly larger than the real distance value. Extinction values were found [E21]

in the given direction in which the studied stellar systems are located. The relation between distance modulus and the distance of the star is supplemented by extinction.

$$m - M = -5 + 5 \log d + A_V. \quad (5.4)$$

GX Lac

The spectral type of GX Lac is B5 (Cannon & Pickering 1993). The primary star effective temperature T_1 was estimated at 15 000 K based on the spectral type. The brightness decrease of the secondary minimum is significantly smaller than the primary. It can be assumed that the secondary component has a smaller radius and lower effective temperature than the primary. The input value for the temperature was selected to be 9 000 K, this value is refined by calculation during the modelling. The phase position of the secondary minimum is not precisely 0.5 but it is in the phase of 0.4985. The difference is 0.0015 in phase. By multiplying by orbital period, the time difference of 0.0095 days is obtained. $O - C$ diagram of GX Lac shows that the stars trajectories are ellipses. The vertical shift of the secondary minima corresponds with the time difference obtained from the phase position. Both the light curve and $O - C$ diagram confirmed that the system eccentricity is non-zero. The elliptical trajectories are probably close to the circles according to the light curve. The secondary minima are lower on the $O - C$ diagram, which corresponds to that argument of periastron $\omega = 180$ deg.

The radial velocity curve contains only the primary component. Absolute radii, masses, and the component distance a could not be determined accurately. Inclination angle, the temperature of the secondary component, and relative radii (to the distance a) can be determined from the light curve. Mass ratio q was continuously estimated using an approximate formula by Graczyk (2003):

$$\log L_1 - \log L_2 = \frac{M_{\text{bol}2} - M_{\text{bol}1}}{2.5}, \quad \log q = \frac{\log L_2 - \log L_1}{3.664}. \quad (5.5)$$

L_1 and L_2 are approximate star luminosities, which were calculated from absolute bolometric magnitudes $M_{\text{bol}1}$ and $M_{\text{bol}2}$. These magnitudes were obtained from PHOEBE calculations.

Absolute parameters of the components were estimated from the table of Majaek [E22]. First, the parameters for the calculated temperatures were found. Furthermore, the ratio of masses and radii from PHOEBE and the table were compared. Parameter $q = 0.46$ estimation is in good agreement with the table ($q = 0.50$). Radii ratio of calculated model $R_1/R_2 \approx 1.79$. The ratio in the table is about 1.63. Approximate values of masses and radii were selected with respect

to the modelling (see Table 5.1). Using these estimates of absolute radii and knowledge of relative radii, the distance between the components was approximately determined at $34 R_{\odot}$. PHOEBE calculation from radial velocity curve shown, that the distance value is about $17 R_{\odot}$. However, this is the value determined from the primary star, which is approximately twice as mass as the secondary component. The distance estimation would therefore be twice this value.

The calculated and estimated parameters are summarized in Table 5.1. The PHOEBE model fits well with the observations. There is a slight difference between model and secondary minimum in TESS data. The results can be compared with Svechnikov & Kuznetsova (2004), where there are only some approximate values of some parameters. The distance estimation 1140 pc agrees with the literature (Gaia et al. 2018, Bailer-Jones et al. 2018, Gaia Collaboration 2020, Bailer-Jones et al. 2021). The uncertainty of the distance is relatively large because the absolute parameters were only estimated.

Table 5.1: Parameters of GX Lac.

Parameter	Value	Error
T_1 [K]	15 000	500
T_2 [K]	9 900	500
R_1 [R_{\odot}]	3.3	0.3
R_2 [R_{\odot}]	2.1	0.3
M_1 [M_{\odot}]	4.6	0.3
M_2 [M_{\odot}]	2.3	0.3
q	0.46	0.10
i [deg]	86.8	0.1
a [R_{\odot}]	34	5
e	0.002	0.001
v_{cent} [km s^{-1}]	-8	10
$\log g_1$	3.8	0.2
$\log g_2$	3.9	0.2
A_V [mag]	1.87	0.11
L_1 [L_{\odot}]	500	70
L_2 [L_{\odot}]	40	10
M_{V1} [mag]	-1.98	0.20
M_{V2} [mag]	0.71	0.20
d [pc]	1 140	200

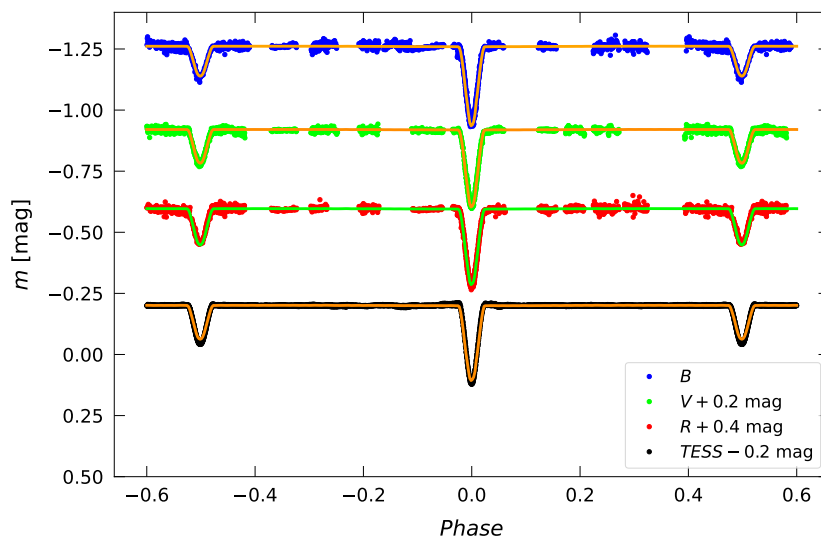


Figure 5.15: Phase light curve model of GX Lac.

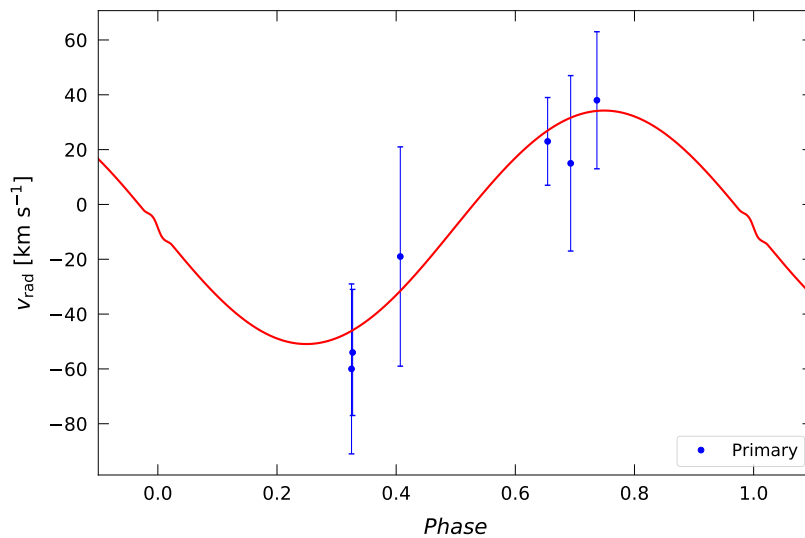


Figure 5.16: Radial velocity curve of GX Lac. There is only the primary component. Synthetic curve is for the components distance $17 R_{\odot}$.

TT Lyr

Minima depths on the light curve of TT Lyr are very various in different colours. It indicates that the components have significantly different effective temperatures. The primary minimum has the largest decrease in blue colour and the smallest in the filter *I*. The depth of the secondary minimum is, however, smallest in the blue filter and largest in the *I* filter. Therefore, it can be concluded that the primary component is a hot star with a high effective temperature. Temperature estimation $T_1 = 20\,000$ K was done based on the spectral type. The secondary component temperature is substantially smaller, its initial value for modelling was 4800 K. Liao & Qian (2010) stated that the spectral type of the secondary component is K0 and the mass ratio $q = 0.27$. Probably no total eclipses occur. The inclination angle is near to 80 deg. Circular trajectories were assumed for both stars.

The system brightness is changing between the eclipses. The changes are approximately symmetrical concerning the primary minimum. There is a possibility that one component filled its Roche lobe completely or for the most part. Brancewicz & Dworak (1980) estimated that the filling rate of the Roche lobe for the secondary component is approximately 85 %. Furthermore, there is an estimation that the secondary component has a larger radius but smaller mass than the primary. Giuricin & Mardirossian (1981) and Svechnikov & Kuznetsova (2004) also stated that the secondary component of TT Lyr has a larger radius and q is about 0.3. It can be concluded that the mass transfer from the originally more massive star to the less massive occurred during the stars life. Algol paradox is probably observed.

The model assumes that one component (secondary) has already completely filled its Roche lobe. The system is therefore semidetached. Final parameters from the modelling are summarized in Table 5.2. The model relatively matches with the assumptions from the literature. The distance between the components has a relatively large uncertainty due to the small number of radial velocities of the primary component. The distance to the Earth 3300 pc was calculated from the model parameters. The distance from publications is around 1500 pc (Cruzalebes et al. 2019, Gaia et al. 2018, Bailer-Jones et al. 2018, Gaia Collaboration 2020, Bailer-Jones et al. 2021). This contradiction can be due to the different effective temperature of the primary component or different morphology of the system.

Table 5.2: Parameters of TT Lyr.

Parameter	Value	Error
T_1 [K]	20 000	500

Table 5.2 (continued)

Parameter	Value	Error
T_2 [K]	5 500	500
R_1 [R_\odot]	3.8	0.2
R_2 [R_\odot]	7.2	0.2
M_1 [M_\odot]	7.7	0.2
M_2 [M_\odot]	1.2	0.2
q	0.25	0.05
i [deg]	82.1	0.3
a [R_\odot]	27	5
v_{cent} [km s^{-1}]	3	10
$\log g_1$	4.1	0.1
$\log g_2$	3.0	0.1
A_V [mag]	0.3155	0.0078
L_1 [L_\odot]	2 100	170
L_2 [L_\odot]	43	8
M_{V1} [mag]	-3.53	0.20
M_{V2} [mag]	0.69	0.20
d [pc]	3 300	200

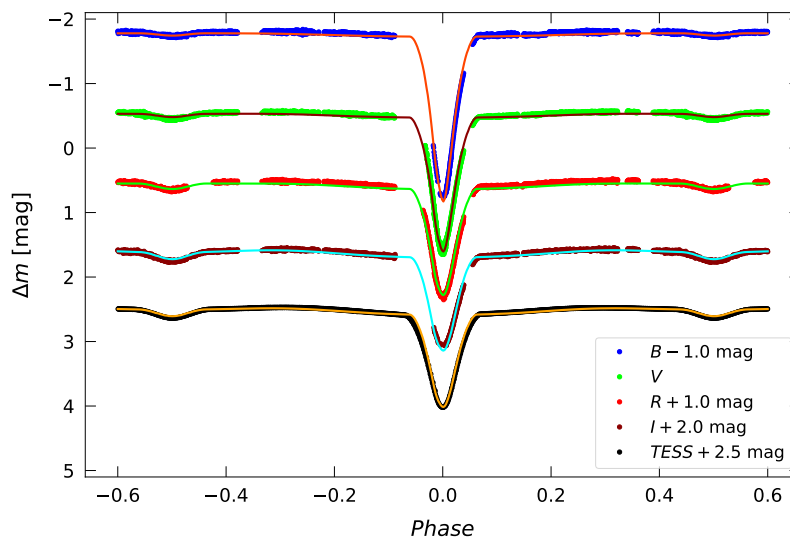


Figure 5.17: Phase light curve model of TT Lyr.

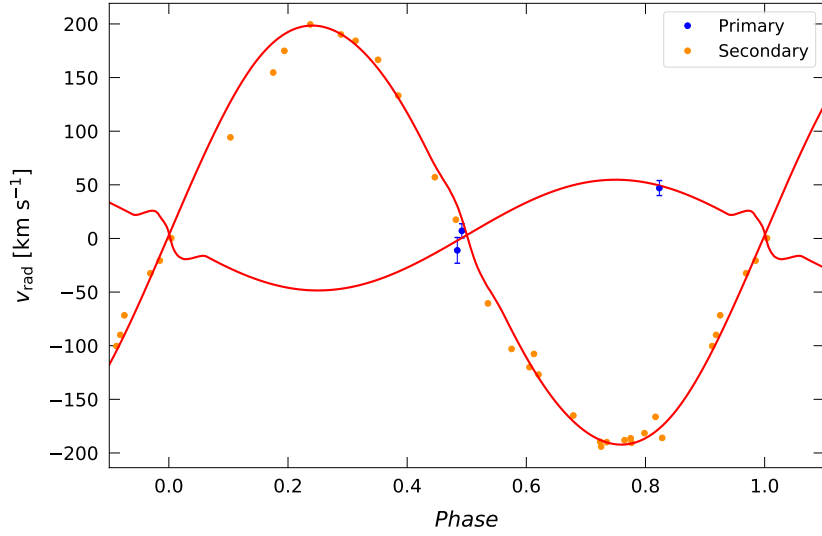


Figure 5.18: Radial velocity curve of TT Lyr.

OGLE LMC-ECL-7641

The effective temperature of the primary component $T_1 = 18\,000$ K was fixed during the modelling. The temperature of the secondary component was 12 000 K in the beginning. The mass ratio is smaller than 1 from the shape of the radial velocity curve. Phase positions of the minima were moving due to the apsidal motion. Due to the large period of apsidal motion, it was not possible to determine how these positions would change over time. MACHO data were used for modelling because contains a sufficient amount of measurements in a short time. The spectra were generated significantly later than the photometric data from MACHO. Therefore, these datasets differ in the argument of periastron. It was therefore necessary to use a different value for the light curve and the radial velocity curve. The values are not known precisely, there were estimations $\omega = 100$ deg for the radial velocity curve and $\omega = 70$ deg for the light curve.

The radial velocities indicate that the system has probably high eccentricity. The modelling of the radial velocities (Figure 5.20) was done without issues. However, the radial velocities of the secondary component in the phase about 0.9 do not fit with the model. The light curve in the primary minimum was not covered well. There are some points, that are probably wrong or influenced by the apsidal motion already within the MACHO observation time interval.

Table 5.3 shows the calculated parameters of the final model. The distance of this binary system is only 17 000 pc. Thus value does not correspond with

the known distance of LMC (Pietrzyński et al. 2019, Elgueta et al. 2016, Taormina et al. 2020, Alves 2004). There is no guarantee that this distance value is real. The distances from the databases (Gaia et al. 2018, Bailer-Jones et al. 2018, Gaia Collaboration 2020, Bailer-Jones et al. 2021) are not very reliable for this star. This could be because the values may not be completely accurate over long distances.

Table 5.3: Parameters of OGLE LMC-ECL-7641.

Parameter	Value	Error
T_1 [K]	18 000	500
T_2 [K]	16 600	500
R_1 [R_\odot]	5.0	0.1
R_2 [R_\odot]	3.4	0.1
M_1 [M_\odot]	6.1	0.1
M_2 [M_\odot]	4.7	0.1
q	0.77	0.05
i [deg]	84.0	0.3
a [R_\odot]	32	2
e	0.31	0.03
v_{cent} [km s^{-1}]	-8	10
$\log g_1$	3.8	0.1
$\log g_2$	4.0	0.1
A_V [mag]	1.87	0.23
L_1 [L_\odot]	2 400	350
L_2 [L_\odot]	800	100
M_{V1} [mag]	-3.66	0.20
M_{V2} [mag]	-2.47	0.20
d [kpc]	17	2

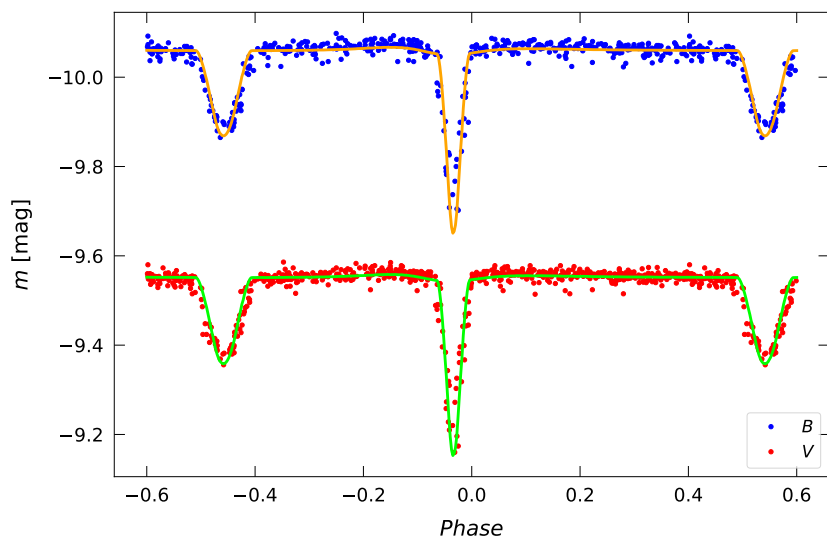


Figure 5.19: Phase light curve model of OGLE LMC-ECL-7641.

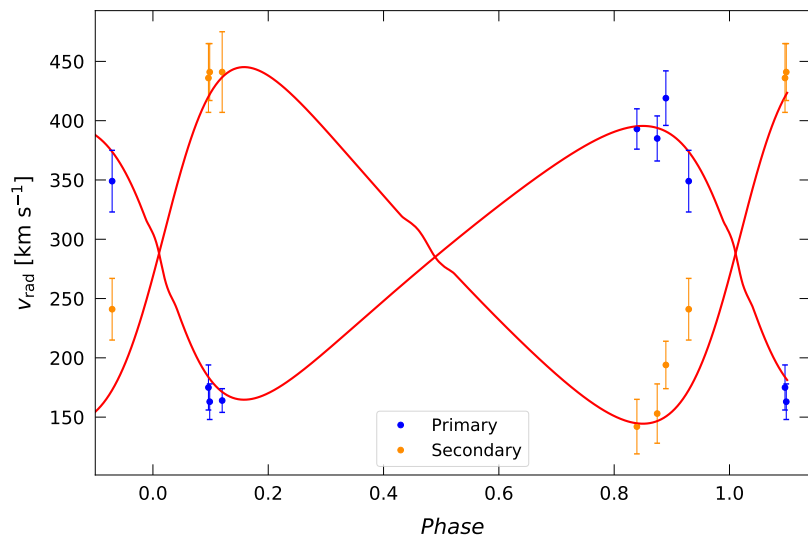


Figure 5.20: Radial velocity curve of OGLE LMC-ECL-7641.

OGLE LMC-ECL-17660

The light curves from MACHO were used for OGLE LMC-ECL-17660 modelling. The data cover well the whole orbital cycle. The apsidal motion could not be calculated, because its period is too long. The spectral type of this system is not precisely known. It was determined from the spectra. There are mainly lines of hydrogen and neutral helium. Using the presence of certain spectral lines, an estimate of the spectral type between B2 and B5 was made. The corresponding effective temperature interval is between 14 000 K and 22 000 K. Furthermore, color index $V - I = -0.181$ mag from OGLE was used to estimate the effective temperature T_1 . From [E16] table the temperature is between 16 000 K and 17 500 K. The temperature of the primary component for modelling was estimated to 18 000 K.

The argument of periastron could not be determined precisely. However, its estimation could be done. From the observation time of MACHO, the value is more than 90 deg. The estimated value was 110 deg. The stars have elliptical trajectories according to the $O - C$ diagram. The ellipses could be very close to the circles according to the radial velocity curve. The curve also shows that the secondary component is more massive than the primary.

Both minima are very similar. The input value of T_2 was 17 000 K. Light curve and radial velocity curve contain a sufficient amount of data for precise modelling of absolute parameters (Table 5.4). The model fits well with the measurements.

The calculated distance value is $44\,000 \pm 5\,000$ pc. Compared to the available literature (Gaia et al. 2018, Bailer-Jones et al. 2018, Gaia Collaboration 2020, Bailer-Jones et al. 2021), this value slightly differs. However, the estimation in the mentioned sources could be inaccurate. It is therefore possible to conclude that OGLE LMC-ECL-17660 is in this dwarf galaxy, probably in the front region of the view from our Galaxy.

Table 5.4: Parameters of OGLE LMC-ECL-17660.

Parameter	Value	Error
T_1 [K]	18 000	500
T_2 [K]	17 400	500
R_1 [R_\odot]	6.6	0.1
R_2 [R_\odot]	7.3	0.1
M_1 [M_\odot]	9.2	0.2
M_2 [M_\odot]	11.0	0.2
q	1.2	0.1
i [deg]	88.0	0.2
a [R_\odot]	39	1

Table 5.4 (continued)

Parameter	Value	Error
ω [deg]	110	10
e	0.10	0.1
v_{cent} [km s $^{-1}$]	268	10
$\log g_1$	3.8	0.1
$\log g_2$	3.8	0.1
A_V [mag]	1.066	0.340
L_1 [L_{\odot}]	4 130	250
L_2 [L_{\odot}]	4 360	260
M_{V1} [mag]	-4.27	0.20
M_{V2} [mag]	-4.33	0.20
d [kpc]	44	5

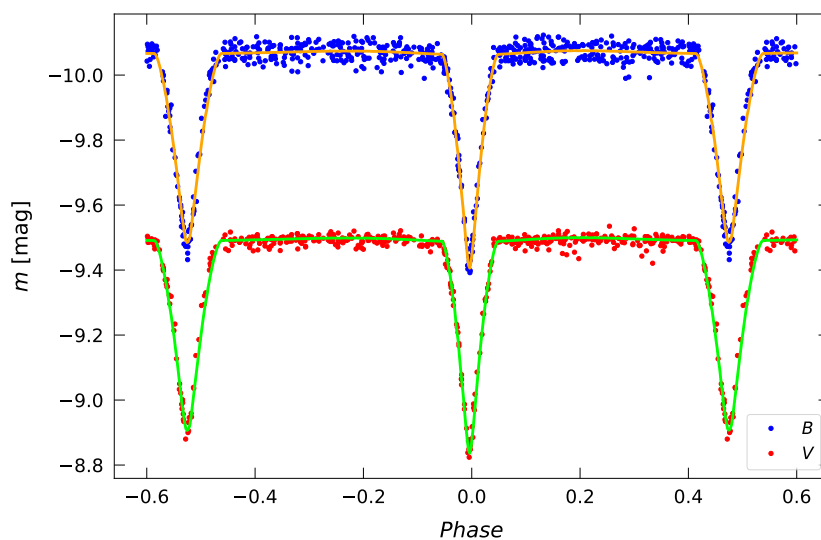


Figure 5.21: Phase light curve model of OGLE LMC-ECL-17660.

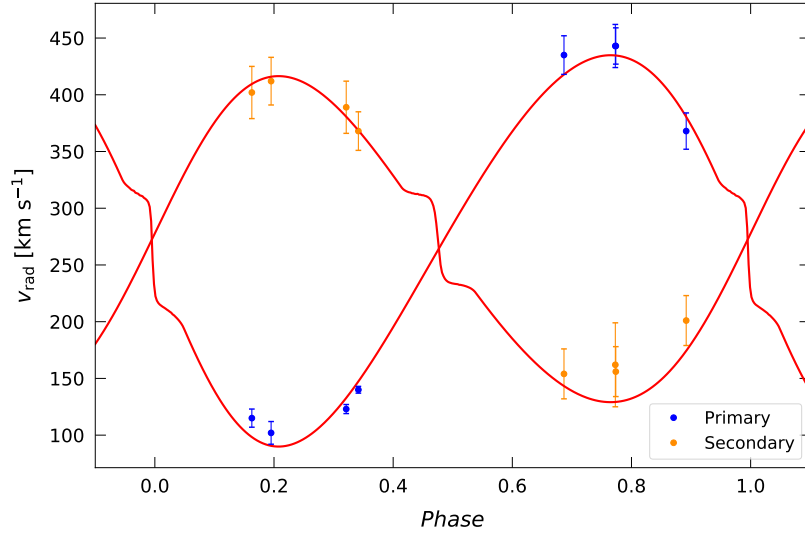


Figure 5.22: Radial velocity curve of OGLE LMC-ECL-17660.

5.5 Discussion

The period analysis was done for all four eclipsing systems. Data fitting and ephemeris correction could be possible for GX Lac and TT Lyr. $O - C$ diagrams for LMC stars showed a more complex course of changes. They were not fitted due to the short observation time. The modelling was complicated for some parts. There was a lack of high-resolution spectral measurements for some stars. The calculated parameters could be expected from the assumptions and literature. Some results of the models differ variously from the available sources. However, a comprehensive analysis has not yet been performed for studied stars, which would include period analysis, modelling, and distance calculation. Precise values for comparison are therefore not completely available.

$O - C$ diagram of GX Lac does not contain a large number of points. Nevertheless, the non-zero eccentricity of the system is evident from these data. The light curve and $O - C$ diagram agree that the secondary minima occur at different times than the system would have zero eccentricity. However, these changes are very small and the trajectories are very close to the circles.

The light curve covers well the course of brightness changes in all used colours. The parameters from the light curve can be determined well. The radial velocity curve contains only one component. It is impossible to precisely calculate some quantities, especially radii and masses due to the lack of the radial velocity data.

In addition, the calculated radial velocities have large uncertainties due to the nature of the hydrogen lines in the spectra.

The final model and the calculated quantities can correspond to reality. Even though the sizes and masses were only estimated from the table, it can be assumed that these values are close to the actual parameters of the stars. The calculated distance matches the already available sources. The error was calculated taking into account the circumstances of the parameter estimates. However, it can be slightly overestimated.

TT Lyr is a long known variable star. Its $O - C$ diagram contains a large amount of data. However the visual observations which do not correspond well with new CCD and photoelectric data needs more careful and detailed analysis. The available secondary minima are slightly different from the primary and not sufficient for analysis. Further observations of them would help to clarify this task.

The model fits quite well the data. The parameters have quite real values according to the temperatures and evolutionary status of the stars. The distance is more than twice as large as the values in the listed sources. If the distance of 1 500 pc from the catalogues is assumed the luminosity will be about $330 L_{\odot}$. This value is smaller compared to the model and the literature. It is therefore possible that the distance may be larger than 1 500 pc.

A possible explanation for this contradiction may be due to an inaccurate estimate of the primary component effective temperature. The system also does not have to be semidetached, but detached, where the secondary component does not fill its Roche lobe completely. The known distance values are only from catalogues, there was no targeted research to determine the distance of this binary system. Therefore, the actual distance may be different. Further research and modelling could solve this distance problem. The spectra of the primary component, from which the radial velocities and the effective temperature would be determined, would help to clarify the distance value.

The apsidal motion of OGLE LMC-ECL-7641 strongly influences the minima positions on the phase light curve over time. The modelling was therefore harder. It was necessary to use the different arguments of periastron ω for the light curve and radial velocity curve. Data indicated non-zero eccentricity, which was confirmed by modelling. Nevertheless, the model does not fit the data precisely. An error may have occurred in determining the wavelengths of the lines that were used to calculate the radial velocity or there could be some other effects.

The light curve fitting corresponds relatively well to the measurement. There are some points with a larger deviation in the region of the primary minimum. The apsidal motion can cause these higher residua or an observation error could have occurred at these points. Similar minor differences between the model and

measurement can be seen around the secondary minimum. The calculated parameters relatively coincide with the predicted values, which can be assumed from both curves.

The model can be compared with the light curve analysis by Zasche et al. (2020). The main difference between this publication is the presence of the third body. The final model in this work does not count with another object. Probably due to this fact, some parameters are different, especially the temperature of the secondary component. It was estimated to be more than 19 000 K in the publication. The system eccentricity was very similar. Apsidal motion period is, however, significantly smaller than the estimation based on the $O - C$ diagram. Masses and radii have no comparison.

The result value of the distance $d = 17\,000$ pc is significantly smaller than the LMC distance, which is about 50 000 pc (Pietrzyński et al. 2019, Elgueta et al. 2016, Taormina et al. 2020, Alves 2004). The system should have very different parameters than those which were determined if its distance should be about the distance of the LMC. The effective temperature of the primary component could be higher than the estimated. There is no sufficient number of spectroscopic observations and the calculated radial velocities are not equally distributed on the radial velocity curve. Further future research would be needed to clarify this, which would also help to better determine the period of the apsidal motion.

For the star OGLE LMC-ECL-17660, the apsidal motion was proved using its $O - C$ diagram. It was not consistent to calculate the apsidal motion. Its period is too long and only a small time interval of changes is captured in the $O - C$ diagram. It, therefore, remains a task of further research. The radial velocity curve clearly shows that elliptical trajectories of the stars are close to the circles, but not as similar as for GX Lac.

Due to the apsidal motion, which caused changes in the positions of the minima on the phase curve, not all available data were used. However, MA-CHO measurements were suitable for modelling. The apsidal motion have only negligible influence in the observation time interval. The radial velocity curve covers regions around the velocity amplitudes, which greatly facilitated the system modelling. The final model is probably the first model of this star system. The calculated quantities cannot be compared with other research. The final parameters, however, well correspond with the observations. The system distance corresponds with the distance of the LMC, where the system should be. In contrast to catalogue sources, where the distances of many stars were calculated, this calculation is more realistic and reliable.

Conclusion

Four eclipsing binary systems were studied in this work. Two of them are in our Galaxy and the other two are located in the Large Magellanic Cloud galaxy. The primary components are hot stars of the spectral type B. The systems have orbital periods between 5 and 7 days and all the light curves are of type Algol.

The observations campaign was organized to obtain new photometric data and the phase light curves. Furthermore, photometric observations were adopted from other observers, surveys, and satellites, especially the OGLE survey and TESS satellite. The phase curves were constructed based on these data. The radial velocities of these stars were calculated using the spectral line wavelengths. Other values of the radial velocities were adopted from the known databases.

The period analysis of the systems was performed. Minima were sought in the original publications. Other minima times were taken from the databases and there were also new minima timings from the observations. Some data were not used because they looked suspicious and there was no information about the observations and determination method. $O-C$ diagrams were constructed. The apsidal motion was confirmed for the LMC systems with long periods. The detailed analysis was not possible due to the short time of monitoring these objects. The orbital periods of GX Lac and TT Lyr are constant. The visual observations of TT Lyr were probably influenced by inaccurate ephemeris. New CCD and photoelectric data are more reliable and make it possible to refine the ephemeris value. The star trajectories are ellipses for GX Lac, OGLE LMC-ECL-7641, and OGLE LMC-ECL-17660. The elliptical trajectories are significantly different from the circles only in the OGLE LMC-ECL-7641 system.

The modelling of the light curves and the radial velocity curves were performed in PHOEBE software. The absolute parameters of the stars were determined by the model and the distance of each system was calculated. The models correspond to the measurements. However, there are still unresolved tasks. The spectra of GX Lac contain only the primary component. Therefore, some parameters were only estimated. However, even these estimations can be real and the calculated distance coincides with other sources. TT Lyr model shows

the system is semidetached. However, the system could be also detached. There is a contradiction between calculated distance and known values from the literature.

Modelling of OGLE LMC-ECL-7641 was complicated due to the apsidal motion. The distance of LMC is significantly larger than the estimated distance from the model parameters. Detailed spectral analysis with more data could clarify this contradiction. The components of OGLE LMC-ECL-17660 are very similar. The calculated distance indicates that the system is located in the front region of the LMC.

This is probably the first comprehensive analysis of these four binary systems. The important systems parameters were determined. Nevertheless, several tasks have not yet been explained. I will make efforts to resolve these tasks in the coming years. Newer software will be used and more parameters will be included in the modelling. Above all, new spectral observations and detailed spectra analyses are needed.

Bibliography

- Ahnert, P. (1949), ‘Verbesserte Elemente des Algol-Sterns TT Lyrae’, *Astronomische Nachrichten* **277**(3), 138.
- Alves, D. R. (2004), ‘A review of the distance and structure of the large magellanic cloud’, *New Astronomy Reviews* **48**(9), 659–665.
- Bailer-Jones, C., Rybizki, J., Fouesneau, M., Demleitner, M. & Andrae, R. (2021), ‘Estimating distances from parallaxes. v. geometric and photogeometric distances to 1.47 billion stars in gaia early data release 3’, *The Astronomical Journal* **161**(3), 147.
- Bailer-Jones, C., Rybizki, J., Fouesneau, M., Mantelet, G. & Andrae, R. (2018), ‘Estimating distance from parallaxes. iv. distances to 1.33 billion stars in gaia data release 2’, *The Astronomical Journal* **156**(2), 58.
- Bessell, M. S. (2005), ‘Standard photometric systems’, *Annu. Rev. Astron. Astrophys.* **43**, 293–336.
- Boyle, W. S. & Smith, G. E. (1970), ‘Charge coupled semiconductor devices’, *Bell System Technical Journal* **49**(4), 587–593.
- Brancewicz, H. & Dworak, T. Z. (1980), ‘A catalogue of parameters for eclipsing binaries’, *Acta Astronomica* **30**, 501–524.
- Brunet, J., Imbert, M., Martin, N., Mianes, P., Prévot, L., Rebeiro, E. & Rousseau, J. (1975), ‘Studies of the lmc stellar content. i. a catalogue of 272 new o-b2 stars.’, *Astronomy and Astrophysics Supplement Series* **21**, 109–136.
- Cannon, A. J. & Pickering, E. C. (1993), ‘VizieR Online Data Catalog: Henry Draper Catalogue and Extension (Cannon+ 1918-1924; ADC 1989)’, *VizieR Online Data Catalog* p. III/135A.
- Conti, P., Garmany, C. & Massey, P. (1986a), ‘Studies of massive stars in the magellanic clouds. i-new spectral classifications of ob types in the lmc’, *The Astronomical Journal* **92**, 48–59.

- Conti, P. S., Garmany, C. D. & Massey, P. (1986*b*), ‘Studies of massive stars in the Magellanic Clouds. I. New spectral classifications of OB types in the LMC.’, **92**, 48–59.
- Cruzalebes, P., Petrov, R., Robbe-Dubois, S., Varga, J., Burtscher, L., Allouche, F., Berio, P., Hofmann, K.-H., Hron, J., Jaffe, W. et al. (2019), ‘VizieR on-line data catalog: Mdfc version 10 (cruzalebes+, 2019)’, *VizieR Online Data Catalog* pp. II–361.
- Derekas, A., Kiss, L. & Bedding, T. (2007), ‘Eclipsing binaries in the macho database: New periods and classifications for 3031 systems in the large magellanic cloud’, *The Astrophysical Journal* **663**(1), 249.
- Eggleton, P. (2006), *Evolutionary processes in binary and multiple stars*, Vol. 40, Cambridge University Press.
- Eggleton, P. P. (1983), ‘Approximations to the radii of roche lobes’, *The Astrophysical Journal* **268**, 368.
- Elgueta, S., Graczyk, D., Gieren, W., Pietrzyński, G., Thompson, I., Konorski, P., Pilecki, B., Villanova, S., Udalski, A., Soszyński, I. et al. (2016), ‘The orbital and physical parameters, and the distance of the eclipsing binary system ogle-lmc-ecl-25658 in the large magellanic cloud’, *The Astronomical Journal* **152**(2), 29.
- Faccioli, L., Alcock, C., Cook, K., Prochter, G. E., Protopapas, P. & Syphers, D. (2007), ‘Eclipsing binary stars in the large and small magellanic clouds from the macho project: The sample’, *The Astronomical Journal* **134**(5), 1963.
- Fukugita, M., Shimasaku, K., Ichikawa, T., Gunn, J. et al. (1996), The sloan digital sky survey photometric system, Technical report, SCAN-9601313.
- Gaia, C., Brown, A., Vallenari, A., Prusti, T., De Bruijne, J., Babusiaux, C., Juhász, Á., Marschalkó, G., Marton, G., Molnár, L. et al. (2018), ‘Gaia data release 2 summary of the contents and survey properties’, *Astronomy & Astrophysics* **616**(1).
- Gaia Collaboration (2020), ‘VizieR Online Data Catalog: Gaia EDR3 (Gaia Collaboration, 2020)’, *VizieR Online Data Catalog* p. I/350.
- Giuricin, G. & Mardirossian, F. (1981), ‘Some aspects of mass loss and mass transfer in algol variables’, *The Astrophysical Journal Supplement Series* **46**, 1–26.

- Graczyk, D. (2003), ‘Light-curve solutions for bright detached eclipsing binaries in the Small Magellanic Cloud: absolute dimensions and distance indicators’, *342*(4), 1334–1348.
- Harwood, M. & Shapley, H. (1933), ‘Y Camelopardalis and TT lyrae’, *Annals of Harvard College Observatory* **84**(2), 37–55.
- Hilditch, R. W. (2001), *An introduction to close binary stars*, Cambridge University Press.
- Hoňková, K., Juryšek, J., Lehký, M., Šmelcer, L., Trnka, J., Mašek, M., Urbaník, M., Auer, R., Vrašták, M., Kučáková, H., Ruocco, N., Magris, M., Polák, J., Brát, L., Audejean, M., Banfi, M., Moudrá, M., Lomoz, F., Přibík, V., Dřevěný, R., Scaggianti, F., Kocián, R., Cagaš, P., Poddaný, S., Zíbar, M., Jacobsen, J., Marek, P., Colazo, C., Zardin, D., Sobotka, P., Starzomski, J., Hladík, B., Vincenzi, M., Skarka, M., Walter, F., Chapman, A., Díaz, N. D., Aceti, P., Singh, P., Kalista, L., Kamenec, M., Zejda, M., Marchi, F., Bílek, R., Guzzo, P., Corfini, G., Onderková, K., Hečko, A., Mina, F., Vítek, M., Barsa, R., Quinones, C., Taormina, M., Melia, R., Schneider, M., Scavuzzo, A., Marcionni, N., Ehrenberger, R., Tapia, L., Fasseta, G., Suarez, N., Scaggianti, D., Artusi, E., Garcia, R., Grnja, J., Fišer, A., Hynek, T., Vilášek, M., Rozehnal, J., Kalisch, T., Lang, K., Gorková, S., Novysedlák, R., Salvaggio, F., Smyčka, T., Spurný, M., Wikander, T., Mravik, J., Šuchaň, J. & Čaloud, J. (2013), ‘B.R.N.O. Contributions #38 Times of minima’, *Open European Journal on Variable Stars* **160**, 1.
- Howell, S. B. (2006), *Handbook of CCD astronomy*, Vol. 5, Cambridge University Press.
- Häussler, K. (1980), ‘Mitteilungen der bruno-h.-bürgel-sternearte hartha’.
- Hübscher, J., Steinbach, H.-M. & Walter, F. (2008), ‘BAV-Results of observations - Photoelectric Minima of Selected Eclipsing Binaries and Maxima of Pulsating Stars’, *Information Bulletin on Variable Stars* **5830**, 1.
- Johnson, H. L. & Morgan, W. (1953), ‘Fundamental stellar photometry for standards of spectral type on the revised system of the yerkes spectral atlas’, *The Astrophysical Journal* **117**, 313.
- Keller, S. C. & Wood, P. R. (2002), ‘Large magellanic cloud bump cepheids: probing the stellar mass-luminosity relation’, *The Astrophysical Journal* **578**(1), 144.
- Kolář, J. (2020), ‘Fotometrie těsných dvojhvězd’, *ÚTFA PřF MU, Brno*.

- Kopal, Z. (1955), The classification of close binary systems, in ‘Annales d’Astrophysique’, Vol. 18, p. 379.
- Kreiner, J. M. (1968), ‘On the Variability of the Star BD +56 2855’, *Information Bulletin on Variable Stars* **249**, 1.
- Kwee, K. & Van Woerden, H. (1956), ‘A method for computing accurately the epoch of minimum of an eclipsing variable’, *Bulletin of the Astronomical Institutes of the Netherlands* **12**, 327.
- Lause, F. (1936), ‘Beobachtungen von Bedeckungsveränderlichen VII’, *Astronomische Nachrichten* **259**(12), 189.
- Lause, F. (1938), ‘Beobachtungen von Bedeckungsveränderlichen XI’, *Astronomische Nachrichten* **266**(2), 17.
- Liao, W.-P. & Qian, S.-B. (2010), ‘The most plausible explanation of the cyclic period changes in close binaries: the case of the rs cvn-type binary ww dra’, *Monthly Notices of the Royal Astronomical Society* **405**(3), 1930–1939.
- Liška, J. & Skarka, M. (2015), ‘O-C diagrams and period changes in stellar systems’, *Open European Journal on Variable Stars* **169**, 38–44.
- Mikulášek, Z. (2015), ‘Phenomenological modelling of eclipsing system light curves’, *Astronomy & Astrophysics* **584**, A8.
- Mikulášek, Z., Chrastina, M., Zejda, M., Janík, J., Yhu, L. & Qian, S. (2013), ‘Kwee-van woerden method: To use or not to use?’, *arXiv preprint arXiv:1311.0207*.
- Mikulášek, Z. & Zejda, M. (2013), ‘Úvod do studia proměnných hvězd’.
- Mikulášek, Z., Wolf, M., Zejda, M. & Pecharová, P. (2006), ‘On Methods for the Light Curves Extrema Determination’, **304**(1-4), 363–365.
- Morgan, W. W. & Keenan, P. (1973), ‘Spectral classification’, *Annual Review of Astronomy and Astrophysics* **11**(1), 29–50.
- Munari, U. & Fiorucci, M. (2003), ‘The asiago database on photometric systems’, *Memorie della Societa Astronomica Italiana* **74**, 151.
- Nijland, A. A. (1913), ‘Notizen über Algolsterne’, *Astronomische Nachrichten* **195**, 439.

- Pawlak, M., Soszyński, I., Udalski, A., Szymański, M. K., Wyrzykowski, Ł., Ulaczyk, K., Poleski, R., Pietrukowicz, P., Kozłowski, S., Skowron, D. M., Skowron, J., Mróz, P. & Hamałowicz, A. (2016), ‘The OGLE Collection of Variable Stars. Eclipsing Binaries in the Magellanic System’, **66**(4), 421–432.
- Percy, J. R. (2007), *Understanding variable stars*, Cambridge University Press.
- Pietrzyński, G., Graczyk, D., Gallenne, A., Gieren, W., Thompson, I., Pilecki, B., Karczmarek, P., Górski, M., Suchomska, K., Taormina, M. et al. (2019), ‘A distance to the large magellanic cloud that is precise to one per cent’, *Nature* **567**(7747), 200–203.
- Plavec, M. (1968), ‘Evolution of close binaries of shorter period and moderate mass’, *Astrophysics and Space Science* **1**(2), 239–263.
- Portegies Zwart, S. & Yungelson, L. R. (1998), ‘Formation and evolution of binary neutron stars’, *Astronomy and Astrophysics* **332**, 173–188.
- Prša, A. & Zwitter, T. (2005), ‘A computational guide to physics of eclipsing binaries. i. demonstrations and perspectives’, *The Astrophysical Journal* **628**(1), 426.
- Ribas, I. (2004), Distances and fundamental properties of eclipsing binaries in the lmc and m31, *in* ‘Spectroscopically and Spatially Resolving the Components of the Close Binary Stars’, Vol. 318, pp. 261–269.
- Sabby, J. A., Sandberg Lacy, C. H., Ibanoglu, C. & Claret, A. (2011), ‘Absolute Properties of the Eccentric Eclipsing Binary Star FT Orionis’, **141**(6), 195.
- Samolyk, G. (2013), ‘Recent minima of 273 eclipsing binary stars’, *Javso* **41**, 122.
- Samolyk, G. (2019), ‘Recent minima of 242 eclipsing binary stars’, *Journal of the American Association of Variable Star Observers (JAAVSO)* **47**(1), 106.
- Schmitt, A. R., Hartman, J. D. & Kipping, D. M. (2019), ‘Lctools: a windows-based software system for finding and recording signals in lightcurves from nasa space missions’, *arXiv preprint arXiv:1910.08034* .
- Sekiguchi, M. & Fukugita, M. (2000), ‘A study of the b- v color-temperature relation’, *The Astronomical Journal* **120**(2), 1072.
- Shapley, H. (1913), *The Orbits of Eighty-seven Eclipsing Binaries:- A Summary*.
- Shapley, M. B. (1917), ‘Lightcurves and orbital elements of TT Lyrae and Y Camelopardalis.’, **46**, 56–63.

- Simon, A., Metlova, N., Godunova, V. & Vasylenko, V. (2019), ‘Spectral classification and estimation of distances to the be/x-ray binaries 1h1936+541 and 1h2202+501’, *Kinematics and Physics of Celestial Bodies* **35**, 38–45.
- Sperlich, K. & Stolz, H. (2013), ‘Quantum efficiency measurements of (em) ccd cameras: high spectral resolution and temperature dependence’, *Measurement Science and Technology* **25**(1), 015502.
- Strömgren, B. (1956), ‘Two-dimensional spectral classification of f stars through photoelectric photometry with interference filters’, *Vistas in Astronomy* **2**, 1336–1346.
- Svechnikov, M. & Kuznetsova, E. F. (2004), ‘VizieR online data catalog: Approximate elements of eclipsing binaries (svechnikov+, 1990)’, *VizieR Online Data Catalog* pp. V–124.
- Taormina, M., Kudritzki, R.-P., Puls, J., Pilecki, B., Sestl, E., Pietrzyński, G., Urbaneja, M. A. & Gieren, W. (2020), ‘Toward early-type eclipsing binaries as extragalactic milestones. ii. nlte spectral analysis and stellar parameters of the detached o-type system ogle-lmc-ecl-06782 in the lmc’, *The Astrophysical Journal* **890**(2), 137.
- Terrell, D. (2001), ‘Eclipsing binary stars: Past, present, and future’, *Journal of the American Association of Variable Star Observers (JAAVSO)* **30**(1), 1.
- Torres, G., Lacy, C. H., Marschall, L. A., Sheets, H. A. & Mader, J. A. (2006), ‘The eclipsing binary v1061 cygni: Confronting stellar evolution models for active and inactive solar-type stars’, *The Astrophysical Journal* **640**(2), 1018.
- Trypsteen, M. F. & Walker, R. (2017), *Spectroscopy for amateur astronomers: recording, processing, analysis and interpretation*, Cambridge University Press.
- Uitterdijk, J. (1934), ‘The eclipsing star 62.1933 lacertae, a binary with apsidal motion’, *Bulletin of the Astronomical Institutes of the Netherlands* **7**, 159.
- Wells, D. C. & Greisen, E. W. (1979), Fits-a flexible image transport system, in ‘Image Processing in Astronomy’, p. 445.
- Wilson, R. E. (1979), ‘Eccentric orbit generalization and simultaneous solution of binary star light and velocity curves’, *The Astrophysical Journal* **234**, 1054–1066.
- Wilson, R. E. & Devinney, E. J. (1971), ‘Realization of accurate close-binary light curves: application to mr cygni’, *The Astrophysical Journal* **166**, 605.

Wright, C. O., Egan, M. P., Kraemer, K. E. & Price, S. D. (2003), ‘The Tycho-2 Spectral Type Catalog’, **125**(1), 359–363.

Zasche, P., Wolf, M., Kučáková, H., Kára, J., Merc, J., Zejda, M., Skarka, M., Janík, J. & Kurfürst, P. (2020), ‘First apsidal motion and light curve analysis of 162 eccentric eclipsing binaries from lmc’, *Astronomy & Astrophysics* **640**, A33.

Zhu, L.-Y., Zejda, M., Mikulášek, Z., Liška, J., Qian, S.-B. & de Villiers, S. N. (2012), ‘The photometric study of a neglected near contact binary: Bs vulpeculae’, *The Astronomical Journal* **144**(2), 37.

Electronic Sources

- [E1] <https://www.bav-astro.eu/index.php/veroeffentlichungen/lichtenknecker-database/lkdb-b-r>
- [E2] <http://var2.astro.cz/ocgate/index.php?lang=en>
- [E3] <https://sites.uni.edu/morgans/astro/course/Notes/section2/spectraltemps.html>
- [E4] <https://www.osapublishing.org/oe/fulltext.cfm?uri=oe-26-26-34131&id=403158#g001>
- [E5] <http://simbad.u-strasbg.fr/simbad/>
- [E6] <https://www.aavso.org/>
- [E7] <https://astro.physics.muni.cz/en/observatory/>
- [E8] <https://www.eso.org/public/teles-instr/lasilla/danish154/>
- [E9] <https://stelweb.asu.cas.cz/slechta/2m/>
- [E10] <https://www.eso.org/sci/facilities/paranal/instruments/uves.html>
- [E11] <http://dr4.lamost.org/>
- [E12] <http://dr5.lamost.org/>
- [E13] <http://dr5.lamost.org/http://star-www.dur.ac.uk/~pdraper/splat/splat-vo/splat-vo.html>
- [E14] <https://amper.physics.muni.cz/>
- [E15] <https://github.com/HinataSoft/Silicups>

- [E16] <http://var2.astro.cz/index.php>
- [E17] <http://ooruri.kusastro.kyoto-u.ac.jp/pipermail/vsnet-ecl/>
- [E18] <https://projects.iq.harvard.edu/dasch>
- [E19] <https://docs.lightkurve.org/>
- [E20] <https://www.sdss.org/dr16/irspec/>
- [E21] <https://irsa.ipac.caltech.edu/applications/DUST/>
- [E22] http://www.pas.rochester.edu/emamajek/EEM_dwarf_UBVIJHK_colors_Teff.txt
- [E23] <https://aladin.u-strasbg.fr/>

Available to 4 June 2021.

Appendices

Table A.1: Minima times of GX Lac.

Time (HJD)	Error	Type	Detector	Observer	Method
2455351.5172	0.0002	p	V	M. Zejda	AMPER
2456495.4607	0.0005	p	V	R. Auer	AMPER
2457963.5203	0.0004	p	BVRI	M. Zejda	AMPER
2458319.41457	0.0003	p	BVR	J. Kolář	AMPER
2458373.42536	0.0004	s	BVR	J. Kolář	AMPER
2458389.32157	0.0002	p	BVR	J. Kolář	AMPER
2458802.41371	0.0002	p	BVR	J. Kolář	AMPER
2458818.29423	0.0004	s	BVR	J. Kolář	AMPER
2457194.541	0.001	p	V	M. Zejda	AMPER
2458370.26178	0.0006	p	BVR	J. Kolář	AMPER
2458408.38714	0.002	p	BVR	J. Kolář	AMPER
2458786.51700	0.002	s	BVR	J. Kolář	AMPER
2458719.79554	0.0003	p	V	G. Samolyk	AMPER
2456101.4343	0.0004	p	CCD	M. Urbaník	bootstrap- ping [E16]
2458748.3838	0.0003	s	CCD	V. Dienstbier	bootstrap- ping [E16]
2457248.550	0.001	s	CCD	L. Šmelcer	bootstrap- ping [E16]
2457245.380	0.001	p	CCD	L. Šmelcer	bootstrap- ping [E16]
2439749.3973	X	p	photoelec- tric	J.M. Kreiner	X

Table A.1 (continued)

Time (HJD)	Error	Type	Detector	Observer	Method
2445189.486	0.003	p	photoelec- tric	J.M. Kreiner	tracing paper
2445993.413	0.005	s	photoelec- tric	J.M. Kreiner	tracing paper
2446009.312	0.003	p	photoelec- tric	J.M. Kreiner	tracing paper
2454366.4544	0.0013	p	CCD	F. Agerer	X
2455097.3028	0.0011	p	CCD	F. Agerer	X
2456568.5297	0.008	s	CCD	F. Agerer	X
2456924.4269	X	s	CCD	F. Agerer	X
2455834.5156	0.0002	p	CCD	M. & K.Rätz	X
2456231.711	0.001	s	V	R. Diethelm	X
2458742.0307	0.0002	s	TESS	TESS	SILICUPS
2458745.216	0.001	p	TESS	TESS	SILICUPS
2458748.3851	0.0003	s	TESS	TESS	SILICUPS
2458754.7424	0.0002	s	TESS	TESS	SILICUPS
2458757.9275	0.0002	p	TESS	TESS	SILICUPS
2458761.09817	0.00025	s	TESS	TESS	SILICUPS
2458767.45166	0.00025	s	TESS	TESS	SILICUPS
2458770.6364	0.0002	p	TESS	TESS	SILICUPS
2458773.8070	0.0002	s	TESS	TESS	SILICUPS
2458780.1617	0.0002	s	TESS	TESS	SILICUPS
2458783.3470	0.0002	p	TESS	TESS	SILICUPS
2458786.5167	0.0003	s	TESS	TESS	SILICUPS

Table A.2: Minima times of TT Lyr.

Time (HJD)	Error	Type	Detector	Observer	Method
2458688.7573	0.0004	p	TESS	TESS	SILICUPS
2458694.0007	0.0005	p	TESS	TESS	SILICUPS
2458699.2450	0.0005	p	TESS	TESS	SILICUPS
2458704.4885	0.0008	p	TESS	TESS	SILICUPS
2458709.731	0.001	p	TESS	TESS	SILICUPS
2457519.4050	0.0005	p	CCD	M. Urbaník	AMPER
2459071.5528	0.0002	p	CCD	R. Auer	AMPER

Table A.2 (continued)

Time (HJD)	Error	Type	Detector	Observer	Method
2459082.0374	0.001	p	CCD	H. Itoh, R. Auer	AMPER
2411610.562	X	p	photo-graphic	M. Harwood	X
2412727.469	X	p	photo-graphic	M. Harwood	X
2414856.437	X	p	photo-graphic	M. Harwood	X
2414866.893	X	p	photo-graphic	M. Harwood	X
2414903.603	X	p	photo-graphic	M. Harwood	X
2415123.845	X	p	photo-graphic	M. Harwood	X
2415632.505	X	p	photo-graphic	M. Harwood	X
2415653.48	X	p	photo-graphic	M. Harwood	X
2415658.701	X	p	photo-graphic	M. Harwood	X
2415978.594	X	p	photo-graphic	M. Harwood	X
2416083.482	X	p	photo-graphic	M. Harwood	X
2416245.999	X	p	photo-graphic	M. Harwood	X
2416261.744	X	p	photo-graphic	M. Harwood	X
2416366.605	X	p	photo-graphic	M. Harwood	X
2416403.335	X	p	photo-graphic	M. Harwood	X
2416733.667	X	p	photo-graphic	M. Harwood	X
2416754.66	X	p	photo-graphic	M. Harwood	X

Table A.2 (continued)

Time (HJD)	Error	Type	Detector	Observer	Method
2416817.567	X	p	photo-graphic	M. Harwood	X
2416927.706	X	p	photo-graphic	M. Harwood	X
2417079.779	X	p	photo-graphic	M. Harwood	X
2418233.396	X	p	photo-graphic	M. Harwood	X
2418238.625	X	p	photo-graphic	M. Harwood	X
2418458.843	X	p	photo-graphic	M. Harwood	X
2418516.533	X	p	photo-graphic	M. Harwood	X
2418579.468	X	p	photo-graphic	M. Harwood	X
2418584.716	X	p	photo-graphic	M. Harwood	X
2418626.654	X	p	photo-graphic	M. Harwood	X
2418904.557	X	p	photo-graphic	M. Harwood	X
2418925.562	X	p	photo-graphic	M. Harwood	X
2418930.786	X	p	photo-graphic	M. Harwood	X
2418946.557	X	p	photo-graphic	M. Harwood	X
2418988.485	X	p	photo-graphic	M. Harwood	X
2419114.32	X	p	visual	S. Enebo	X
2419140.565	X	p	visual	A.A. Nijland	X
2419156.264	X	p	visual	A.A. Nijland	X
2419161.513	X	p	visual	A.A. Nijland	X

Table A.2 (continued)

Time (HJD)	Error	Type	Detector	Observer	Method
2419182.491	X	p	visual	A.A. Nijland	X
2419224.439	X	p	visual	A.A. Nijland	X
2419229.701	X	p	visual	A.A. Nijland	X
2419245.424	X	p	visual	A.A. Nijland	X
2419266.408	X	p	visual	A.A. Nijland	X
2419308.35	X	p	visual	A.A. Nijland	X
2419444.69	X	p	visual	A.A. Nijland	X
2419523.33	X	p	visual	A.A. Nijland	X
2419544.311	X	p	visual	A.A. Nijland	X
2419549.578	X	p	visual	A.A. Nijland	X
2419596.752	X	p	visual	A.A. Nijland	X
2419612.478	X	p	visual	A.A. Nijland	X
2419617.718	X	p	visual	A.A. Nijland	X
2419633.465	X	p	visual	A.A. Nijland	X
2419670.166	X	p	visual	A.A. Nijland	X
2419680.648	X	p	visual	A.A. Nijland	X
2419759.314	X	p	visual	A.A. Nijland	X
2419879.88	X	p	visual	A.A. Nijland	X

Table A.2 (continued)

Time (HJD)	Error	Type	Detector	Observer	Method
2419895.64	X	p	visual	A.A. Nijland	X
2419963.792	X	p	visual	A.A. Nijland	X
2419995.26	X	p	visual	A.A. Nijland	X
2420005.741	X	p	visual	A.A. Nijland	X
2420021.503	X	p	visual	A.A. Nijland	X
2420026.743	X	p	visual	A.A. Nijland	X
2420037.228	X	p	visual	A.A. Nijland	X
2420058.199	X	p	visual	A.A. Nijland	X
2420220.744	X	p	visual	A.A. Nijland	X
2420241.719	X	p	visual	A.A. Nijland	X
2420283.66	X	p	visual	A.A. Nijland	X
2420320.384	X	p	visual	A.A. Nijland	X
2420325.628	X	p	visual	A.A. Nijland	X
2420341.367	X	p	visual	A.A. Nijland	X
2420362.341	X	p	visual	A.A. Nijland	X
2420383.322	X	p	visual	A.A. Nijland	X
2420404.298	X	p	visual	A.A. Nijland	X
2420472.446	X	p	visual	A.A. Nijland	X

Table A.2 (continued)

Time (HJD)	Error	Type	Detector	Observer	Method
2420582.572	X	p	visual	A.A. Nijland	X
2420624.513	X	p	visual	A.A. Nijland	X
2420708.425	X	p	visual	A.A. Nijland	X
2452176.015	X	p	visual	K. Hirosawa	X
2452217.966	X	p	visual	K. Hirosawa	X
2454357.4341	0.0007	p	CCD	H.Jungbluth	X
2439056.222	0.003	p	visual	M.Winiarski	tracing paper
2439622.588	0.008	p	visual	M.Winiarski	tracing paper
2444383.8555	0.0001	p	photoelectric	E.C. Olson	Kwee-van Woerden
2430666.260	X	p	visual	W. Tecza	X
2433440.199	X	p	visual	R. Szafraniec	X
2433571.288	X	p	visual	R. Szafraniec	X
2433896.39	X	p	visual	R. Szafraniec	X
2434132.356	X	p	visual	R. Szafraniec	X
2434216.261	X	p	visual	R. Szafraniec	X
2434976.611	X	p	visual	R. Szafraniec	X
2435338.422	X	p	visual	R. Szafraniec	X
2436308.511	X	p	visual	R. Szafraniec	X
2439035.263	X	p	visual	R. Szafraniec	X
2434011.801	X	p	photographic	G.T. Kowall	X

Table A.2 (continued)

Time (HJD)	Error	Type	Detector	Observer	Method
2434593.82	X	p	photo-graphic	Koch, Koch	X
2437189.393	X	p	photo-graphic	Kühler	X
2437939.349	X	p	photo-graphic	Kühler	X
2438605.2644	X	p	photoelec-tric	K. Walter	X
2439790.355	X	p	visual	K. Locher	X
2442936.582	X	p	visual	K. Locher	X
2444761.396	X	p	visual	K. Locher	X
2444829.578	X	p	visual	K. Locher	X
2445296.264	X	p	visual	K. Locher	X
2446696.333	X	p	visual	K. Locher	X
2447367.536	X	p	visual	K. Locher	X
2447729.373	X	p	visual	K. Locher	X
2448872.505	X	p	visual	K. Locher	X
2449905.499	X	p	visual	K. Locher	X
2450031.351	X	p	visual	K. Locher	X
2450508.543	X	p	visual	K. Locher	X
2450660.589	X	p	visual	K. Locher	X
2450739.275	X	p	visual	K. Locher	X
2451305.564	X	p	visual	K. Locher	X
2451798.475	X	p	visual	K. Locher	X
2452443.426	X	p	visual	K. Locher	X
2452789.547	X	p	visual	K. Locher	X
2453219.545	0.008	p	visual	K. Locher	X
2443041.453	X	p	visual	H. Peter	X
2443665.448	X	p	visual	H. Peter	X
2443707.382	X	p	visual	H. Peter	X
2443749.35	X	p	visual	H. Peter	X
2443791.274	X	p	visual	H. Peter	X
2445191.412	X	p	visual	H. Peter	X
2445212.39	X	p	visual	H. Peter	X
2445275.276	X	p	visual	H. Peter	X
2445296.255	X	p	visual	H. Peter	X
2445621.365	X	p	visual	H. Peter	X

Table A.2 (continued)

Time (HJD)	Error	Type	Detector	Observer	Method
2447063.408	X	p	visual	H. Peter	X
2448222.245	X	p	visual	H. Peter	X
2448442.486	X	p	visual	H. Peter	X
2448484.43	X	p	visual	H. Peter	X
2448505.41	X	p	visual	H. Peter	X
2449947.442	X	p	visual	H. Peter	X
2445925.515	X	p	visual	T.Brelstaff	X
2445275.282	X	p	visual	R.Germann	X
2445296.245	X	p	visual	R.Germann	X
2445946.473	X	p	visual	M. Kohl	X
2456811.4992	0.0002	p	photoelec- tric	F. Agerer	X
2453927.4478	0.0005	p	photoelec- tric	F. Agerer	X
2457199.5345	0.003	p	photoelec- tric	F. Agerer	X
2457928.4153	0.0005	p	photoelec- tric	F. Agerer	X
2427960.48372	X	p	visual	F. Lause	X
2427965.7209	X	p	visual	F. Lause	X
2427976.21621	X	p	visual	F. Lause	X
2427981.48034	X	p	visual	F. Lause	X
2428023.41368	X	p	visual	F. Lause	X
2428107.30393	X	p	visual	F. Lause	X
2428128.26999	X	p	visual	F. Lause	X
2428285.59603	X	p	visual	F. Lause	X
2428364.27464	X	p	visual	F. Lause	X
2428374.73771	X	p	visual	F. Lause	X
2428390.46266	X	p	visual	F. Lause	X
2428427.18285	X	p	visual	F. Lause	X
2428469.15409	X	p	visual	F. Lause	X
2428495.36991	X	p	visual	F. Lause	X
2428532.07068	X	p	visual	F. Lause	X
2428684.12447	X	p	visual	F. Lause	X
2428689.38866	X	p	visual	F. Lause	X
2428752.29869	X	p	visual	F. Lause	X
2428757.55465	X	p	visual	F. Lause	X

Table A.2 (continued)

Time (HJD)	Error	Type	Detector	Observer	Method
2428778.52226	X	p	visual	F. Lause	X
2428820.46873	X	p	visual	F. Lause	X
2428899.10764	X	p	visual	F. Lause	X
2459058.449	0.001	s	CCD	J. Kolář	AMPER
2459100.391	0.002	s	CCD	R. Auer	AMPER
2458686.1415	0.0004	s	TESS	TESS	SILICUPS
2458691.3852	0.0008	s	TESS	TESS	SILICUPS
2458701.8727	0.0008	s	TESS	TESS	SILICUPS
2458707.1154	0.0005	s	TESS	TESS	SILICUPS

Table A.3: Minima times of OGLE LMC-ECL-7641.

Time (HJD)	Error	Type	Observer	Method
2458482.86	0.01	p	M. Zejda	AMPER
2456963.635	0.002	p	M. Zejda.	AMPER
2458122.07	0.01	p	M. Zejda	AMPER
2459185.5187	0.001	p	M. Zejda.	AMPER
2459210.8521	0.001	p	J. Kolář	AMPER
2459248.786	0.002	p	J. Kolář	AMPER
2459188.44	0.01	s	M. Zejda	AMPER
2459213.683	0.002	s	J. Kolář	AMPER
2449266.1190	X	p	X	phase difference
2449512.9515	X	p	X	phase difference
2450760.0519	X	p	X	phase difference
2450968.9573	X	p	X	phase difference
2458482.8687	X	p	X	phase difference
2456963.6349	X	p	X	phase difference
2450316.9107	X	p	X	phase difference
2450538.5531	X	p	X	phase difference
2451848.8243	X	p	X	phase difference
2456602.8701	X	p	X	phase difference
2456349.6074	X	p	X	phase difference
2459210.8461	X	p	X	phase difference
2459210.8593	X	p	X	phase difference
2456963.6463	X	p	X	phase difference
2456640.7996	X	p	X	phase difference
2456640.8010	X	p	X	phase difference

Table A.3 (continued)

Time (HJD)	Error	Type	Observer	Method
2456640.8040	X	p	X	phase difference
2453304.7789	X	p	X	phase difference
2452994.6194	X	p	X	phase difference
2453051.5823	X	p	X	phase difference
2428034.5925	X	p	X	phase difference
2428762.6195	X	p	X	phase difference
2427800.5067	X	p	X	phase difference
2431332.6265	X	p	X	phase difference
2430680.5751	X	p	X	phase difference
2427547.2177	X	p	X	phase difference
2431845.4125	X	p	X	phase difference
2450144.0919	X	s	X	phase difference
2450212.9508	X	s	X	phase difference
2450731.9970	X	s	X	phase difference
2459213.6801	X	s	X	phase difference
2451934.6739	X	s	X	phase difference
2452995.8302	X	s	X	phase difference
2455510.7919	X	s	X	phase difference
2455548.7608	X	s	X	phase difference
2449466.0028	X	s	X	phase difference
2459213.6836	X	s	X	phase difference
2458175.6156	X	s	X	phase difference
2453105.5615	X	s	X	phase difference
2453320.7298	X	s	X	phase difference
2453706.8171	X	s	X	phase difference
2453776.5848	X	s	X	phase difference
2456023.5605	X	s	X	phase difference
2426570.6315	X	s	X	phase difference
2429102.6175	X	s	X	phase difference
2428906.4406	X	s	X	phase difference
2429229.3190	X	s	X	phase difference
2430672.3802	X	s	X	phase difference
2424462.7762	X	s	X	phase difference

Table A.4: Minima times of OGLE LMC-ECL-17660.

Time (HJD)	Error	Type	Observer	Method
2458873.7460	0.0003	p	M. Zejda	AMPER
2458842.6077	0.0002	p	M. Zejda.	AMPER
2458826.8167	0.0004	s	M. Zejda	AMPER
2459231.7368	0.0003	s	J. Kolář	AMPER
2455659.5214	X	p	X	phase difference
2456238.8396	X	p	X	phase difference
2456039.5105	X	p	X	phase difference
2455883.7733	X	p	X	phase difference
2449829.0809	X	p	X	phase difference
2450128.0809	X	p	X	phase difference
2449312.0426	X	p	X	phase difference
2450726.0613	X	p	X	phase difference
2449312.0426	X	p	X	phase difference
2450402.1622	X	p	X	phase difference
2450047.0874	X	p	X	phase difference
2450427.0734	X	p	X	phase difference
2458842.6028	X	p	X	phase difference
2458842.6066	X	p	X	phase difference
2434393.2717	X	p	X	phase difference
2455861.8054	X	s	X	phase difference
2455942.7964	X	s	X	phase difference
2453687.8487	X	s	X	phase difference
2455886.7407	X	s	X	phase difference
2449097.0305	X	s	X	phase difference
2450841.1766	X	s	X	phase difference
2450349.0552	X	s	X	phase difference
2449209.1581	X	s	X	phase difference
2456297.8225	X	s	X	phase difference
2449209.1581	X	s	X	phase difference
2449234.0820	X	s	X	phase difference
2455562.7828	X	s	X	phase difference
2456727.6452	X	s	X	phase difference
2426977.6152	X	s	X	phase difference
2433150.6324	X	s	X	phase difference

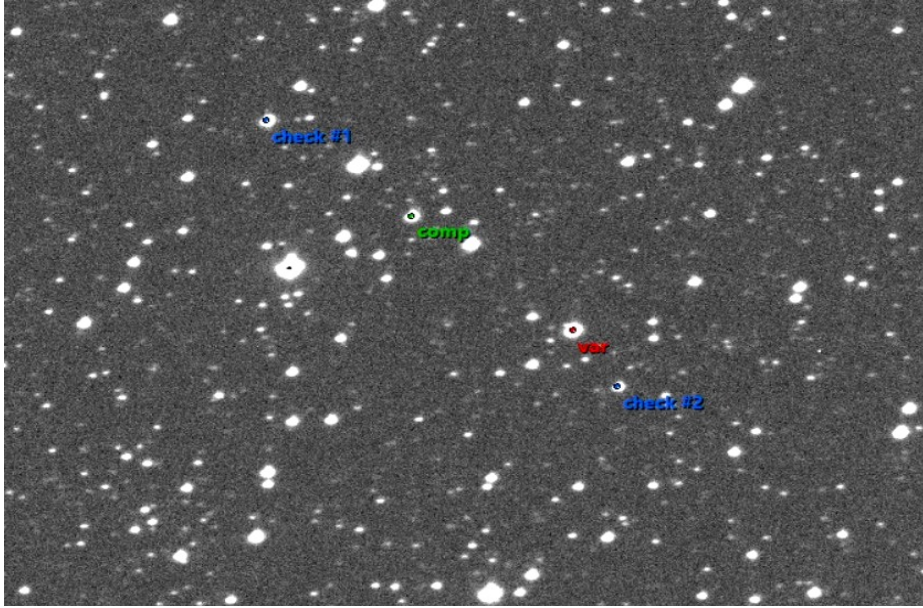


Figure A.1: Map of GX Lac.

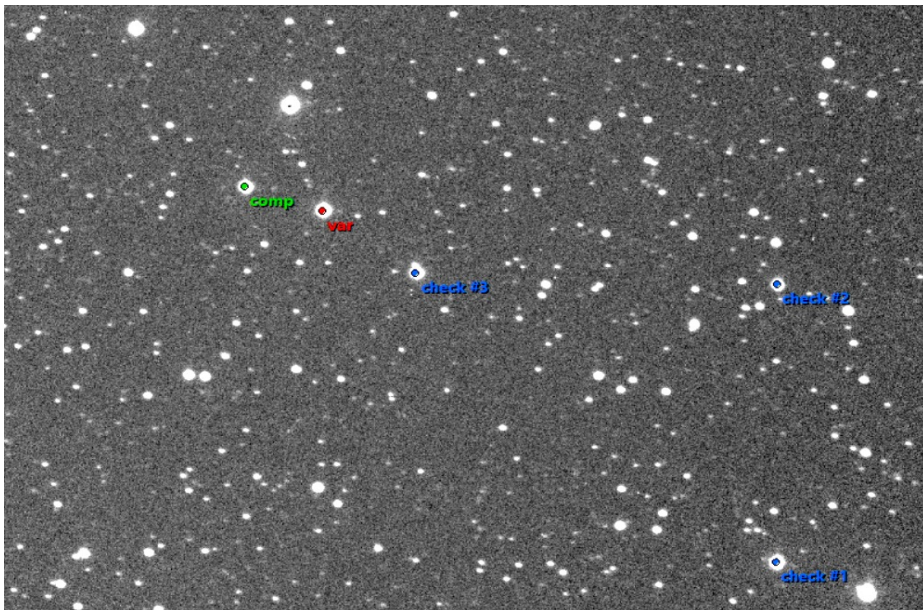


Figure A.2: Map of TT Lyr.

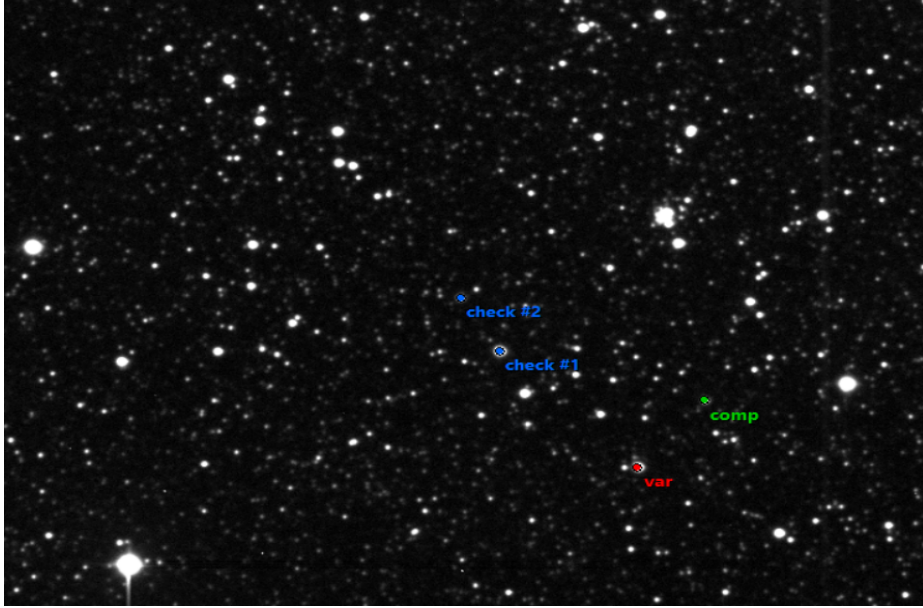


Figure A.3: Map of OGLE LMC-ECL-7641.

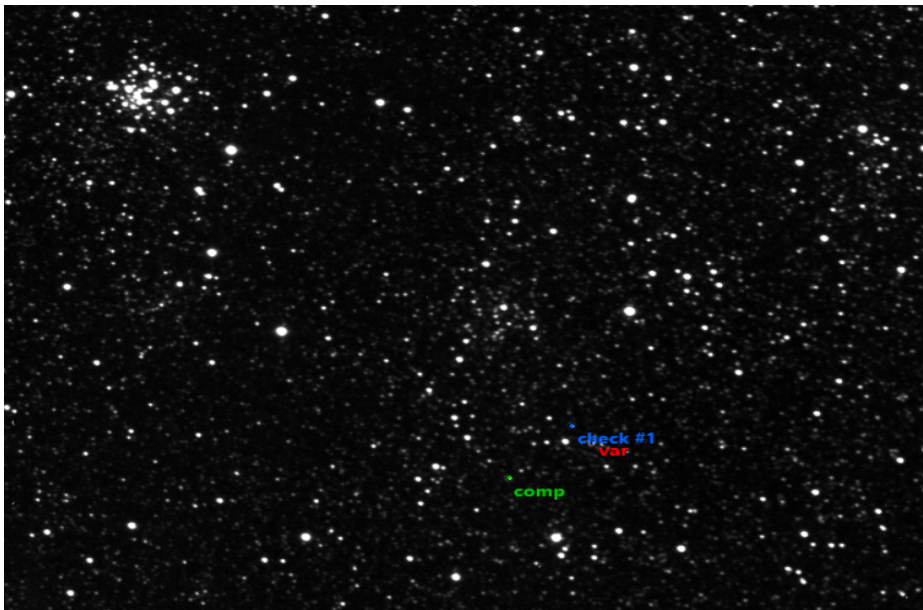


Figure A.4: Map of OGLE LMC-ECL-17660.

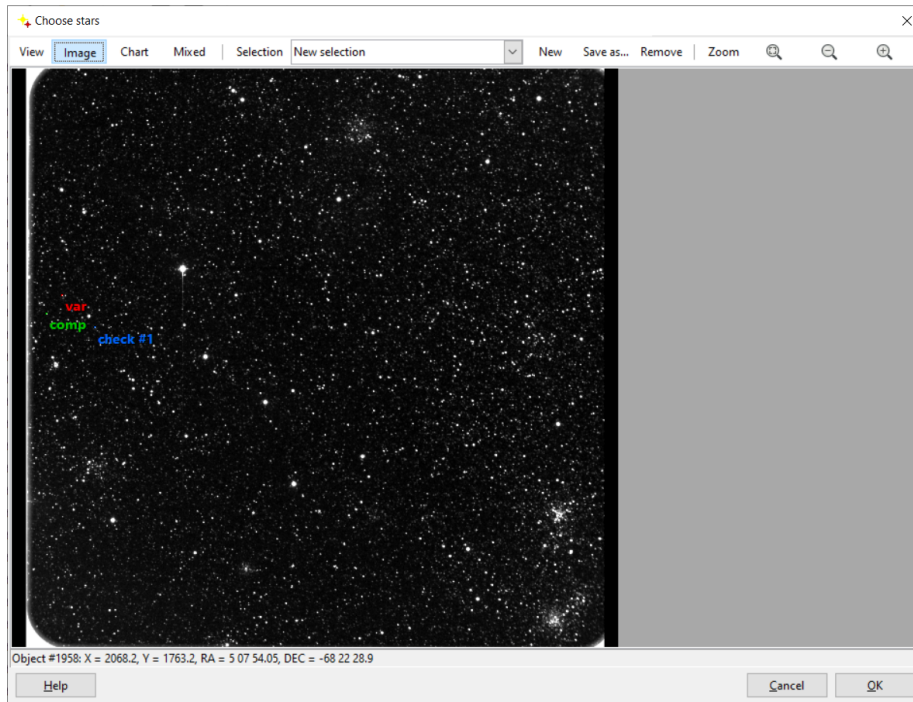


Figure A.5: Selection of the variable, comparison, and check stars in C-Munipack software.

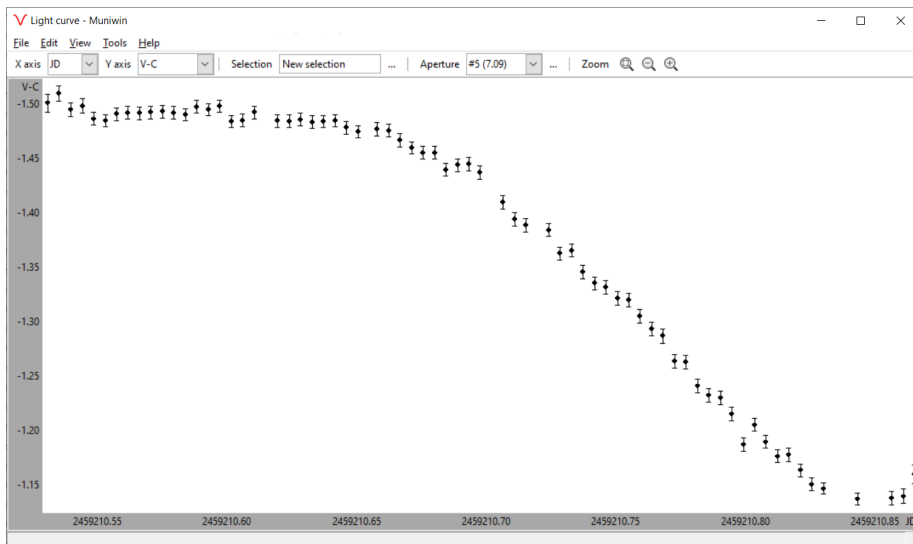


Figure A.6: Obtained light curve of OGLE LMC-ECL-7641 in Munipack software.

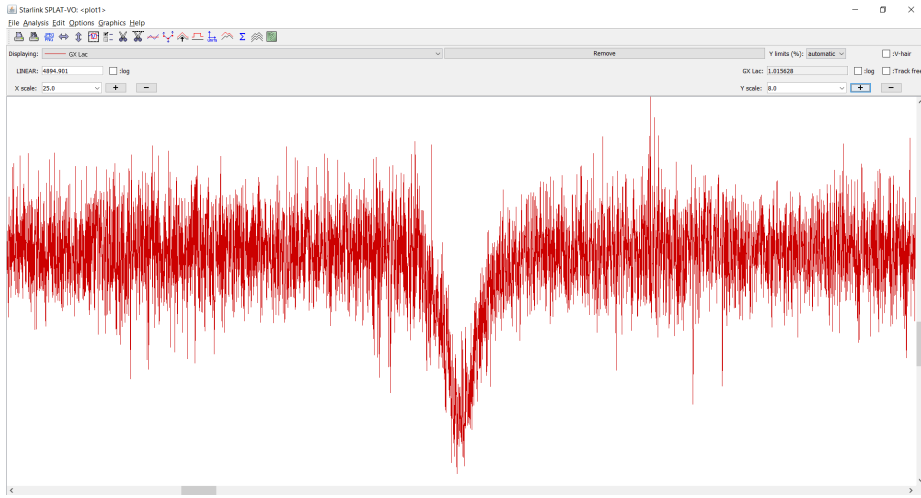


Figure A.7: $H\beta$ line of GX Lac in SPLAT-VO software.

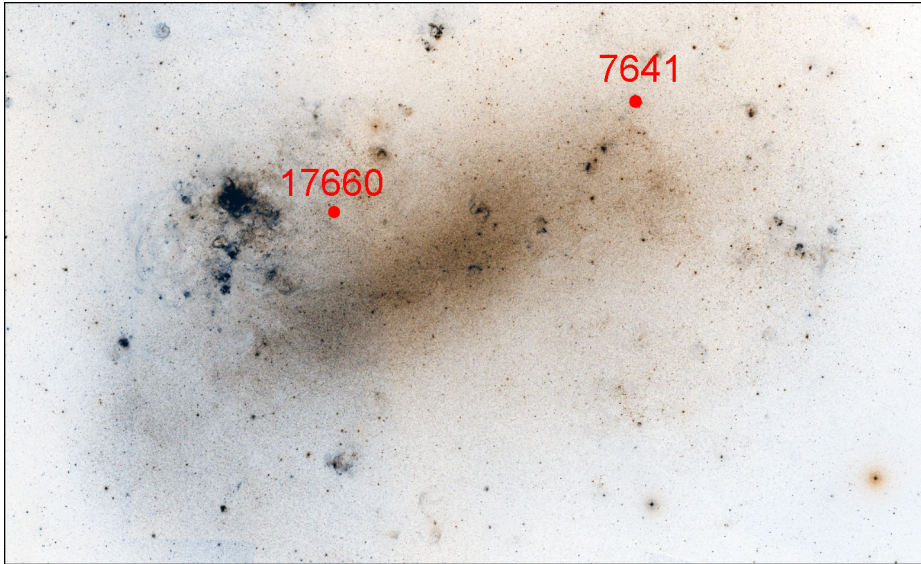


Figure A.8: Map of LMC galaxy and marked positions of studied objects [E23].